## Chevychelov V.Y.[1], Viryus A.A.[2] Partition of fluorine and chlorine between biotite, apatite and melt of water-saturated rare-metal biotite granite. *UDC 550.42*

[1] Korzhinskii Institute of Experimental Mineralogy of RAS; Russia, Chernogolovka, Moscow district [2] Institute of Geology of Ore Deposits, Petrography, Mineralogy and Geochemistry of RAS; Russia, Moscow chev@iem.ac.ru, allavirus@yandex.ru

**Abstract.** Crystallization of liquidus biotite and apatite from a melt of rare-metal granites at water-saturated conditions at pressure of approximately 100 MPa and temperature of 750°C was experimentally studied, depending on the fluorine and chlorine contents in the system. The melts obtained by melting of biotite granites of the Khangilai massif (Eastern Transbaikalia) and an aqueous solutions of acids and salts (1M HF + 1M HCl; 2M HF + 2M KF; 5M HF + 1M HCl) were used in the experiments. The starting weight ratio of solution/granite glass was 1/10. During the first day the experiments were carried out at 830°C (above liquidus temperature), and then the temperature was decreased below the liquidus to 750°C. The total duration of the experiments ranged from 10 to 14 days.

After the experiments were determined the chemical compositions of crystallizing biotite, apatite, and coexisting granite melt, as well as their fluorine and chlorine contents, depending on the initial fluorine and chlorine contents of the system. Fluorine/chlorine ratios in the coexisting phases were calculated. The results were compared with the compositions of biotite and apatite from natural granites of the Khangilai massif.

***Keywords***: *partition; fluorine; chlorine; biotite; apatite; crystallization of granite melt; experiment*

**Introduction.** The crystallization of liquidus biotite and apatite from the melt of rare-metal granites at water-saturated conditions was experimentally studied depending on the content of fluorine and chlorine in the system at pressure of about 100 MPa and temperature of 750°C.

**Research methods.** The experiments utilized melts obtained by melting biotite granite from the Khangilai massif (Eastern Transbaikalia) (Table 1) and aqueous solutions of acid-salt mixtures: 1M HF + 1M HCl; 2M HF + 2M KF; 5M HF + 1M HCl.

The initial solution/granite glass weight ratio was 1:10. Granite glass crystallization experiments were conducted in platinum capsules using an internally heated pressure vessel (IHPV). The first day of the experiments was maintained at supraliquidus conditions at $T$ = 830°C, after which the temperature was lowered below the liquidus to 750°C. The total duration of the experiments ranged from 10 to 14 days. Aqueous solutions were added in excess of their maximum solubility in the granite melt. After the experiments, the capsules contained, in addition to solid glass, a free fluid phase, which was not collected for analysis due to its very small quantity.

After the experiments, the compositions of the synthesized phases and granite glasses were analyzed by electron probe microanalysis (EPMA) using energy-dispersive X-ray spectrometer (for major components) and wavelength-dispersive X-ray spectrometer (for F and Cl).

**Table 1.** Chemical composition of the initial granite glass obtained by melting granite from the Khangilai massif ($T$ = 1350°C, $P$ = 0.1 MPa, unwelded capsule, duration 1 day; in wt.%, normalized to 100%, according to EDS data, F and Cl according to wave spectrometer data)

| Experiment number | n[1] | $SiO_2$ | $TiO_2$ | $Al_2O_3$ | $FeO_{tot}$ | MnO | MgO | CaO | $Na_2O$ | $K_2O$ | F | Cl | Total |
|---|---|---|---|---|---|---|---|---|---|---|---|---|---|
| VZ-1 /melt | 20 | 75.7 | 0.2 | 13.7 | 1.3 | 0.1 | 0.4 | 0.8 | 3.7 | 4.0 | 0.10 | 0.00 | 100.0 |

[1] Number of analyses.

**Main results.** The products obtained from the experiments consisted of granite glass and a very small amount (less than 1 vol. %) of crystalline phases (minerals), represented primarily by mica (biotite) and accessory minerals (apatite, zircon, monazite). Crystal sizes typically did not exceed 10-20 μm. Flat biotite crystals in cross section appeared as elongated plates up to 4-5 μm thick.

The chemical compositions of biotite, fluorapatite, and coexisting granite glasses obtained in the experiments are given in Tables 2, 3, and 4. It was found that the fluorine content in biotite is always higher than that in the coexisting granite melt. With an increase in the fluorine content in the melt (in the system as a whole), the fluorine content in biotite also increases (Fig. 1). The fluorine content in fluorapatites synthesized simultaneously with biotite is virtually independent on the fluorine content in the system. Thus, having reached a maximum content of ~ 3.3 wt.% in apatite with a low fluorine content in the melt (0.10 wt.%), it remains at the same level with an increase in fluorine in the melt to ~ 0.46

wt.% (Fig. 1).

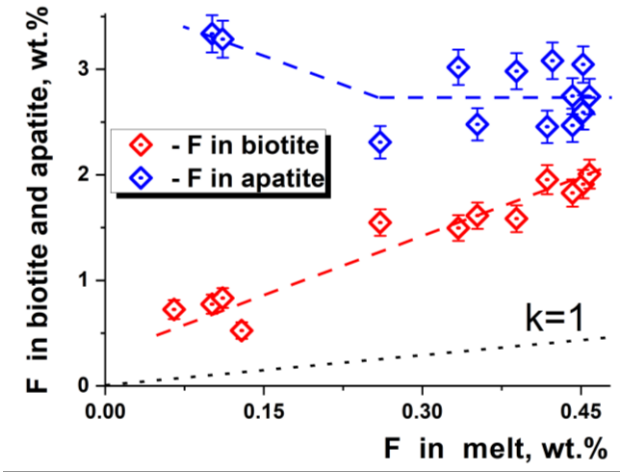


**Fig. 1.** Fluorine content in synthesized biotite and fluorapatite as function of fluorine content in coexisting granite melts. The dotted line (k = 1) corresponds to equal fluorine content in the mineral and melt.

**Table 2.** Chemical composition of synthesized biotites

| Initial solution | Experiment number | $P$, MPa/ $T$, °C | n | $SiO_2$ | $TiO_2$ | $Al_2O_3$ | $FeO_{tot}$ | MnO | MgO | $Na_2O$ | $K_2O$ | F | Cl | Total | F/Cl | $D_F^{Bt/ml}$ [2] | $D_{Cl}^{Bt/ml}$ [2] | Mg# [3] |
|---|---|---|---|---|---|---|---|---|---|---|---|---|---|---|---|---|---|---|
| 1M HF + 1M HCl | VZ-3 /sol-2 | 118/ 750 | 10 | 45.5 | 2.4 | 18.1 | 11.9 | 0.1 | 11.7 | 1.2 | 8.3 | 0.71 | 0.15 | 100.1 | 4.7 | 7.0 | 0.73 | 63.5 |
| 5M HF + 1M HCl | VZ-3 /sol-4 | 118/ 750 | 10 | 46.8 | 1.5 | 17.1 | 8.6 | 0.0 | 14.2 | 1.3 | 8.4 | 1.83 | 0.10 | 99.8 | 19 | 4.2 | 0.47 | 74.6 |
| 5M HF + 5M HCl | VZ-3 /sol-1 | 118/ 750 | 3 | 43.0 | 1.9 | 18.5 | 5.5 | 0.1 | 18.8 | 0.9 | 8.9 | 2.21? | 0.13? | 99.9 | 17? | 2.0? | 0.24? | 85.6 |
| 2M HF + 2M KF | VZ-3 /sol-3 | 118/ 750 | 10 | 46.7 | 2.6 | 15.2 | 11.7 | 0.2 | 12.3 | 1.0 | 8.7 | 1.65 | 0.04 | 100.1 | 37 | 4.8 | - | 64.9 |

[1] Number of analyses. [2] Fluorine and chlorine partition coefficients between biotite and granite melt. [3] Mg# value of biotite, equal to the 100×Mg/(Mg+Mn+Fe) mole ratio in biotite.

**Table 3.** Chemical composition of synthesized fluorapatites

| Initial solution | Experiment number | $P$, MPa/ $T$, °C | n [1] | CaO | $FeO_{tot}$ | $P_2O_5$ | F | Cl | Total | F/Cl | $D_F^{Ap/ml}$ [2] | $D_{Cl}^{Ap/ml}$ [2] |
|---|---|---|---|---|---|---|---|---|---|---|---|---|
| 1M HF + 1M HCl | VZ-3/ sol-2 | 118/ 750 | 2 | 53.5 | 2.3 | 40.7 | 3.31 | 0.14 | 100.0 | 24 | 33 | 0.67 |
| 5M HF + 1M HCl | VZ-3/ sol-4 | 118/ 750 | 7 | 56.1 | 0.0 | 41.0 | 2.80 | 0.11 | 100.0 | 26 | 6.4 | 0.55 |
| 2M HF + 2M KF | VZ-3/ sol-3 | 118/ 750 | 2 | 55.1 | 0.0 | 42.2 | 2.57 | 0.00 | 99.9 | - | 7.6? | - |

[1] Number of analyses. [2] Partition coefficients of fluorine and chlorine between apatite and granite melt.

**Table 4.** Chemical composition of granite glasses coexisting with synthesized minerals

| Initial solution | Experiment number | *P*, MPa/ *T*, °C | n[1] | $SiO_2$ | $Al_2O_3$ | $FeO_{tot}$ | MgO | CaO | $Na_2O$ | $K_2O$ | F | Cl | Total | F/Cl |
|---|---|---|---|---|---|---|---|---|---|---|---|---|---|---|
| 1M HF + 1M HCl | VZ-3 /sol-2 | 118/ 750 | 4 | 75.1 | 14.7 | 0.8 | 0.3 | 0.5 | 3.4 | 5.1 | 0.10 | 0.21 | 100.2 | 0.49 |
| 5M HF + 1M HCl | VZ-3 /sol-4 | 118/ 750 | 6 | 74.3 | 15.0 | 0.4 | 0.3 | 0.9 | 3.8 | 4.7 | 0.44 | 0.20 | 100.0 | 2.15 |
| 5M HF + 5M HCl | VZ-3 /sol-1 | 118/ 750 | 4 | 74.7 | 14.7 | 0.3 | 0.5 | 0.7 | 3.1 | 4.4 | 1.09 | 0.54 | 100.0 | 2.0 |
| 2M HF + 2M KF | VZ-3 /sol-3 | 118/ 750 | 4 | 75.6 | 13.8 | 0.6 | 0 | 0.5 | 3.4 | 5.7 | 0.34 | 0.00 | 99.9 | - |

[1] Number of analyses.

The dependences of the F/Cl ratios in biotite and apatite on the F/Cl ratios in the coexisting granite melt (Fig. 2) are similar in shape to the dependences on the F contents, which is associated with the practically identical (0.20 – 0.21 wt.%) chlorine content in the system.

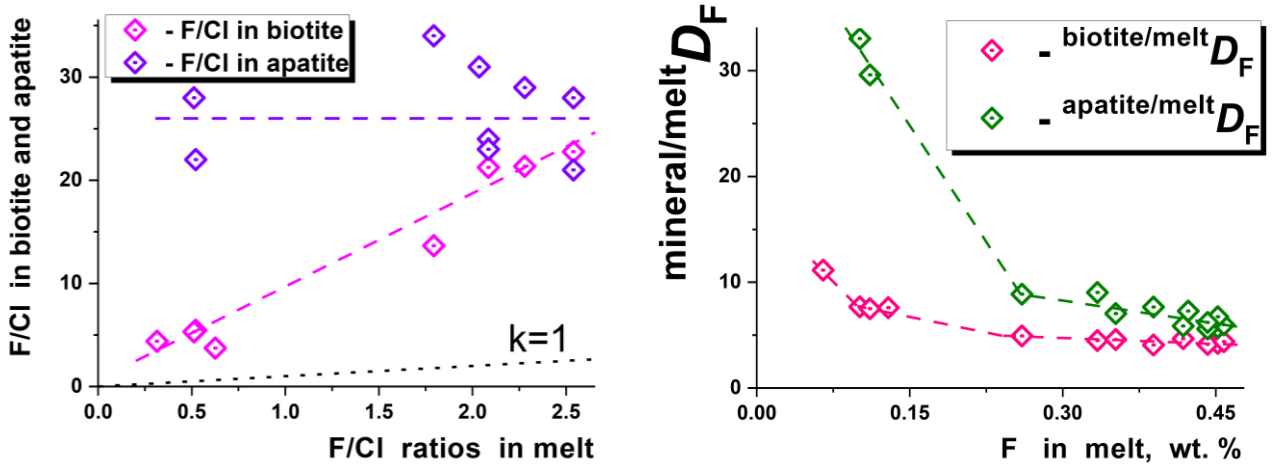





**Fig. 2.** F/Cl ratios in the composition of synthesized biotite and fluorapatite as a function of the F/Cl ratio in coexisting granitic melts. The dotted line (k = 1) corresponds to equality of the F/Cl ratios in the mineral and melt.

**Fig. 3.** Dependence of the partition coefficient of F between the mineral (biotite or fluorapatite) and the coexisting granite melt on the F content in this melt.

The fluorine partition coefficient between biotite and melt ($^{biotite/melt}D_F$) increases significantly (from 4.5 to 7.5–11) with decreasing fluorine content in the melt (Fig. 3). At these conditions, the fluorine partition coefficient between apatite and melt ($^{apatite/melt}D_F$) increases significantly more (from 5.5–9 to 30–33).

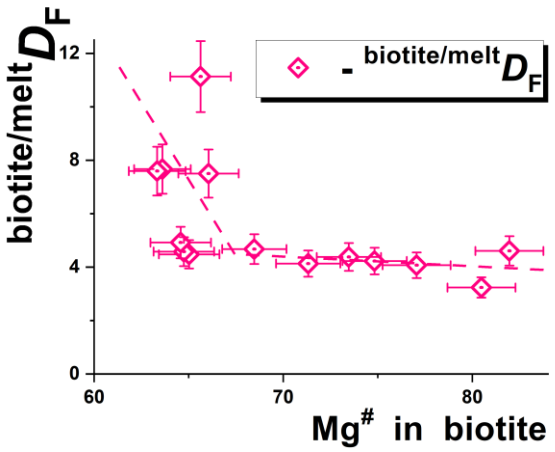


**Fig. 4.** Dependence of the partition coefficient of F between the synthesized biotite and the coexisting granite melt on $Mg^{\#}$ value of this biotite.

$Mg^{\#}$ value of the synthesized biotites (equal to the 100×Mg/(Mg+Mn+Fe) mole ratio) varies in the range from 63.3 to 85.6 and is noticeably higher than the $Mg^{\#}$ value of natural biotites of the Khangilai massif (32.5 – 57.8). The high $Mg^{\#}$ value of the synthesized biotites is apparently associated with a partial loss of iron from the melt into the walls of the platinum capsule during the experiments. The fluorine partition coefficient between biotite and melt ($^{biotite/melt}D_F$) slightly increases with a decrease in the $Mg^{\#}$ value of biotite in the range of 82 – 68 (Fig. 4), but with a further decrease in $Mg^{\#}$ value from ~ 68 to ~ 63.5, the fluorine partition coefficient increases significantly (by 2-3 times from 4.5 to 7.5 – 11).

**Comparison (matching) of the compositions of experimental and natural minerals.** The chemical compositions of experimentally obtained biotites and fluorapatites are compared with those of natural biotites and apatites from granites of the Khangilai massif (Tables 5 and 6). Due to the very low chlorine contents (0.02-0.07 wt.%, close to the detection limit) in natural biotites and the absence of chlorine in natural fluorapatites, this paper compares data on the content and partition coefficients of fluorine only.

**Table 5.** Chemical composition of natural biotites 1 from granites of the Khangilai massif

| Components | n [1] | $SiO_2$ | $TiO_2$ | $Al_2O_3$ | $FeO_{tot}$ | MnO | MgO | $K_2O$ | F [2] | Cl [2] | Total | F/Cl [2] | $D_F^{Bt/ml}$ [3] | Mg# [4] |
|---|---|---|---|---|---|---|---|---|---|---|---|---|---|---|
| Biotite 1 | 10 | 38.1 | 3.4 | 17.4 | 24.2 | 0.3 | 5.6 | 9.7 | 1.07-1.77 / 1.39 | 0.02-0.07 / 0.05 | 100.1 | 22-34/ 27 | 10.7-17.7 / 13.9 | 43 |

[1] Number of analyses. [2] Ranges of F, Cl, F/Cl ratio contents and their average values. [3] Fluorine partition coefficients between biotite and granite melt. [4] $Mg^{\#}$ value of biotite, equal to the 100×Mg/(Mg+Mn+Fe) mole ratio.

**Table 6.** Chemical composition of natural fluorapatites from granites of the Khangilai massif

| Components | n [1] | CaO | $P_2O_5$ | F | Cl | Total | $D_F^{Ap/ml}$ [2] |
|---|---|---|---|---|---|---|---|
| Fluorapatite | 11 | 54.6 | 42.2 | 3.21 | 0.00 | 100.0 | 32 |

[1] Number of analyses. [2] Fluorine partition coefficient between apatite and granite melt.

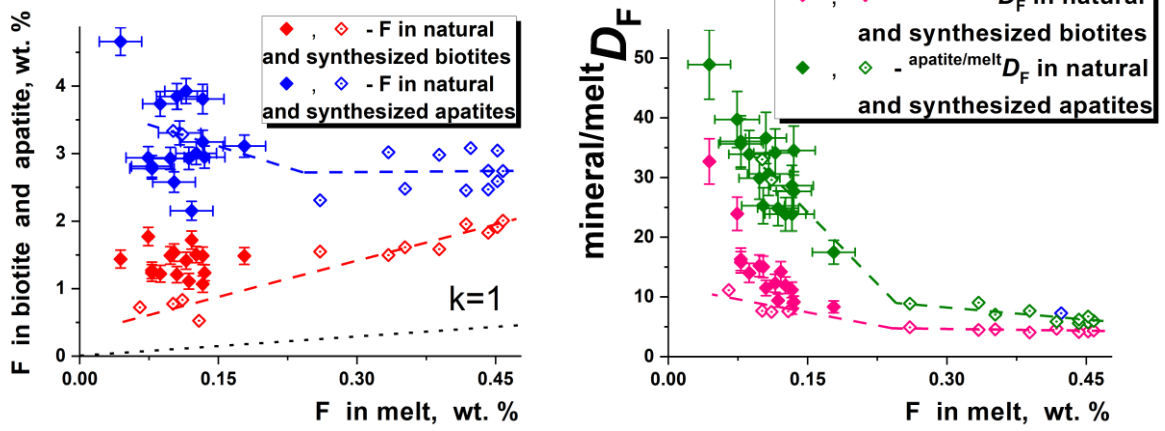


**Fig. 5.** Dependences of F contents in natural and synthesized minerals (biotites and fluorapatites) on F content in granite melts. The dotted line (k = 1) corresponds to equal fluorine contents in the mineral and melt.

**Fig. 6.** Dependences of the partition coefficients of F between natural and synthesized minerals (biotites or fluorapatites) and coexisting granite melts on the F content in this melts.

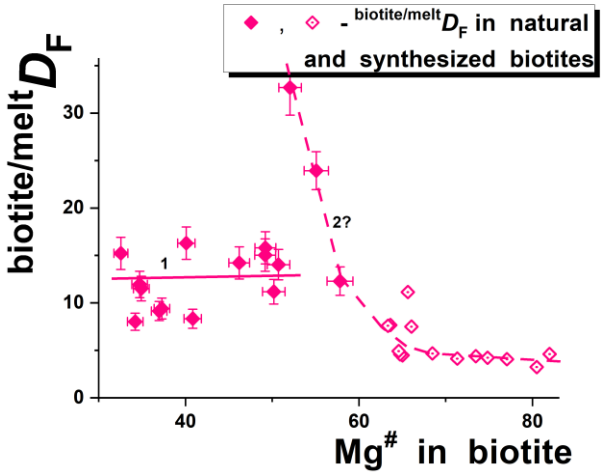


**Fig. 7.** Comparison of the partition coefficients of F between natural and synthesized biotites and coexisting granite melts depending on the $Mg^{\#}$ values of this biotites.

Fluorine contents in natural biotites are approximately twice those in synthesized minerals (Fig. 5). At the same time, fluorine contents in natural fluorapatite are virtually identical to experimental minerals, likely due to the fact that both natural and synthesized fluorapatites are close to saturation in fluorine content. Similar relationships were obtained by comparing the fluorine partition coefficients ($^{mineral/melt}D_F$) between minerals and coexisting granite melts (Fig. 6).

The dependences of the fluorine partition coefficients ($^{biotite/melt}D_F$) on $Mg^{\#}$ values of biotite show approximately three times higher partition coefficients for natural biotites with lower $Mg^{\#}$ values (Fig. 7, dependence 1), however, in this diagram, dependence 2? can also be distinguished, which is expressed in a sharp increase in the fluorine partition coefficients from ~ 8-11 to ~ 33 with a relatively small decrease in the $Mg^{\#}$ values from ~ 63 to ~ 52. The reason for this dependence is still unclear to us; additional research is required to confirm it and clarify the cause.

***Funding.*** *This study is fulfilled under financial support of the project of the Ministry of Education and Science of Russia, project No. 13.1902.24.44, agreement No. 075-15-2024-641.*

## Chevychelov V.Y.[1], Viryus A.A.[2] Influence of temperature on the conditions of formation and composition of biotite crystallizing from granite melt. *UDC 550.42*

[1] Korzhinskii Institute of Experimental Mineralogy of RAS; Russia, Chernogolovka, Moscow district [2] Institute of Geology of Ore Deposits, Petrography, Mineralogy and Geochemistry of RAS; Russia, Moscow chev@iem.ac.ru, allavirus@yandex.ru

**Abstract.** The effect of temperatures ranging from 750°C to 620°C at a pressure of 110–120 MPa on the composition and formation conditions of biotite crystallizing from granite melt was experimentally studied, depending on the fluorine and chlorine content in the system. The melts of biotite granites of the Khangilai massif (Eastern Transbaikalia) and aqueous solutions of acids of the following concentrations (5M HF + 5M HCl; 1M HF + 1M HCl; 5M HF + 1M HCl) were used in the experiments. The starting weight ratio of solution/granite glass was approximately 1/10. During the first day the experiments were carried out at 830°C (above liquidus temperature), and then the temperature was decreased below the liquidus and the experiments were continued at one from three temperatures: 750°C, 720°C, and 620°C. The total duration of the experiments ranged from 10 to 14 days.

The obtained results were compared with the compositions of biotites and contents of fluorine and chlorine of biotites from natural granites of the Khangilai massif.

***Keywords****: influence of temperature; biotite; crystallization of granite melt; partition; fluorine; chlorine; experiment*

**Introduction.** The effect of temperature changes in the range from 750°C to 620°C at pressure of 110–120 MPa on the composition of biotite crystallizing from a rare-metal granite melt at water-saturated conditions was experimentally studied, depending on the fluorine and chlorine content in the system.

**Research methods.** The experiments were carried out using melts obtained by melting biotite granite from the Khangilai massif (Eastern Transbaikalia) (Table 1) and aqueous solutions of acid mixtures: 1M HF + 1M HCl; 5M HF + 1M HCl.

**Table 1.** Chemical composition of the initial granite glass obtained by melting granite from the Khangilai massif ($T$ = 1350°C, $P$ = 0.1 MPa, unwelded capsule, duration 1 day; in wt.%, normalized to 100%, according to EDS data, F and Cl according to wave spectrometer data)

| Experiment number | n[1] | $SiO_2$ | $TiO_2$ | $Al_2O_3$ | $FeO_{tot}$ | MnO | MgO | CaO | $Na_2O$ | $K_2O$ | F | Cl | Total |
|---|---|---|---|---|---|---|---|---|---|---|---|---|---|
| VZ-1 /melt | 20 | 75.7 | 0.2 | 13.7 | 1.3 | 0.1 | 0.4 | 0.8 | 3.7 | 4.0 | 0.10 | 0.00 | 100.0 |

[1] Number of analyses.

The initial solution/granite glass weight ratio was 1/10. Granite glass crystallization experiments were conducted in platinum capsules using an internally heated pressure vessel (IHPV). During the first day the experiment was maintained at supraliquidus conditions at $T$ = 830°C, then the temperature was dropped below the liquidus, and the experiment was continued at one of three temperatures: 750°C, 720°C, and 620°C. The total duration of the experiments ranged from 10 to 14 days. Aqueous solutions were added in excess of their maximum solubility in the granite melt. After the experiments, in addition to solid glass, a free fluid phase was present in the capsules; which was not collected for analysis due to its very small quantity.

After the experiments, the compositions of the synthesized phases and granite glasses were analyzed by electron probe microanalysis (EPMA) using energy-dispersive X-ray spectrometer (for major components) and wavelength-dispersive X-ray spectrometer (for F and Cl).

**Main results.** The experimental products contained very small amounts of crystalline phases (less than 1 vol. %), represented primarily by mica (biotite) (Table 2). Crystal sizes typically did not exceed 10-20 μm. Flat biotite crystals in cross section appeared as elongated plates up to 4-5 μm thick (Fig. 1). The underlying mass containing the crystals was granite glass. The compositions of the granite glasses coexisting with the biotite crystals are given in Table 3.

It was shown that biotites crystallizing in experiments with less HF-rich initial solution of 1M HF + 1M HCl are enriched in FeO (8.8 - 13.6 wt.%), $TiO_2$ (1.7 - 2.4 wt.%) and depleted in MgO (11.1 - 14.2 wt.%), F (0.71 - 3.86? wt.%), compared to experiments with more HF-rich solution of 5M HF + 1M HCl, respectively, in FeO (7.5 - 10.6 wt.%), $TiO_2$ (1.3 - 1.5 wt.%), MgO (14.2 - 17.5 wt.%) and F (1.83 - 5.29? wt.%) (Table 2). Thus, in these experiments, a negative correlation is observed between the Fe and Ti contents and the Mg and F contents in the biotite composition.

**Table 2.** Chemical compositions of synthesized biotites

| Initial solution | Experiment number | $P$, MPa/ $T$, °C | n | $SiO_2$ | $TiO_2$ | $Al_2O_3$ | $FeO_{tot}$ | MnO | MgO | $Na_2O$ | $K_2O$ | F | Cl | Total | F/Cl | $D_F^{Bt/ml}$[2] | $D_{Cl}^{Bt/ml}$[2] | Mg#[3] |
|---|---|---|---|---|---|---|---|---|---|---|---|---|---|---|---|---|---|---|
| 1M HF + 1M HCl | VZ-3 /sol-2 | 118/ 750 | 10 | 45.5 | 2.4 | 18.1 | 11.9 | 0.1 | 11.7 | 1.2 | 8.3 | 0.71 | 0.15 | 100.1 | 4.7 | 7.0 | 0.73 | 63.5 |
| | VZ-5 /sol-2 | 110/ 720 | 7 | 48.1 | 2.1 | 15.5 | 8.8 | 0.1 | 14.2 | 1.0 | 7.5 | 2.47 | 0.14 | 99.9 | 17 | 9.8 | 0.63 | 73.9 |

| Initial solution | Experiment number | $P$, MPa/ $T$, °C | n | $SiO_2$ | $TiO_2$ | $Al_2O_3$ | $FeO_{tot}$ | MnO | MgO | $Na_2O$ | $K_2O$ | F | Cl | Total | F/Cl | $D_F$ Bt/ml [2] | $D_{Cl}$ Bt/ml [2] | $Mg^{\#}$ [3] |
|---|---|---|---|---|---|---|---|---|---|---|---|---|---|---|---|---|---|---|
| | VZ-8 /sol-2 | 110/ 620 | 2 | 41.8 | 1.7 | 18.2 | 13.6 | 0.0 | 11.1 | 0.7 | 8.9 | 3.86? | 0.27? | 100.1 | 14? | 16.8? | 1.3? | 59.3 |
| 5M HF + 1M HCl | VZ-3 /sol-4 | 118/ 750 | 10 | 46.8 | 1.5 | 17.1 | 8.6 | 0.0 | 14.2 | 1.3 | 8.4 | 1.83 | 0.10 | 99.8 | 19 | 1.6 | 0.4 | 74.6 |
| | VZ-5 /sol-4 | 110/ 720 | 9 | 47.0 | 1.3 | 14.4 | 7.5 | 0.1 | 15.8 | 1.0 | 7.9 | 4.92 | 0.13 | 100.1 | 37 | 5.0 | 0.57 | 78.7 |
| | VZ-8 /sol-3 | 110/ 620 | 3(2) | 43.9 | 1.5 | 12.3 | 10.6 | 0.1 | 17.5 | 0.5 | 8.1 | 5.29? | 0.16? | 100.0 | 34? | 4.7? | 0.73? | 74.3 |

[1] Number of analyses. [2] Fluorine and chlorine partition coefficients between biotite and granite melt. [3] $Mg^{\#}$ value of biotite, equal to the 100×Mg/(Mg+Mn+Fe) mole ratio in biotite.

**Table 3.** Chemical composition of granite glasses coexisting with synthesized biotite crystals

| Initial solution | Experiment number | $P$, MPa / $T$, °C | n [1] | $SiO_2$ | $Al_2O_3$ | $FeO_{tot}$ | MgO | CaO | $Na_2O$ | $K_2O$ | F | Cl | Total | F/Cl |
|---|---|---|---|---|---|---|---|---|---|---|---|---|---|---|
| 1M HF + 1M HCl | VZ-3 /sol-2 | 118/ 750 | 4 | 75.1 | 14.7 | 0.8 | 0.3 | 0.5 | 3.4 | 5.1 | 0.10 | 0.21 | 100.2 | 0.49 |
| | VZ-5 /sol-2 | 110/ 720 | 11 | 76.6 | 13.8 | 0.6 | 0.2 | 0.9 | 3.2 | 4.3 | 0.25 | 0.23 | 100.1 | 1.1 |
| | VZ-8 /sol-2 | 110/ 620 | 2 | 75.1 | 14.6 | 0.6 | 0.2 | 0.8 | 3.7 | 4.4 | 0.23? | 0.20? | 99.8 | 1.2? |
| 5M HF + 1M HCl | VZ-3 /sol-4 | 118/ 750 | 6 | 73.6 | 14.9 | 0.4 | 0.3 | 0.9 | 3.8 | 4.7 | 1.18? | 0.31? | 100.1 | 3.8? |
| | VZ-5 /sol-4 | 110/ 720 | 10 | 76.2 | 13.7 | 0.6 | 0.2 | 0.8 | 3.1 | 4.2 | 0.99 | 0.23 | 100.0 | 4.3 |
| | VZ-8 /sol-3 | 110/ 620 | 3 | 75.2 | 14.9 | 0.3 | 0.1 | 0.8 | 3.0 | 4.3 | 1.12? | 0.21? | 99.9 | 5.3? |

[1] Number of analyses.

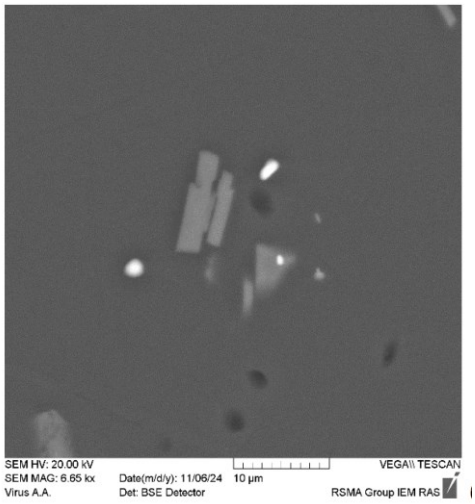


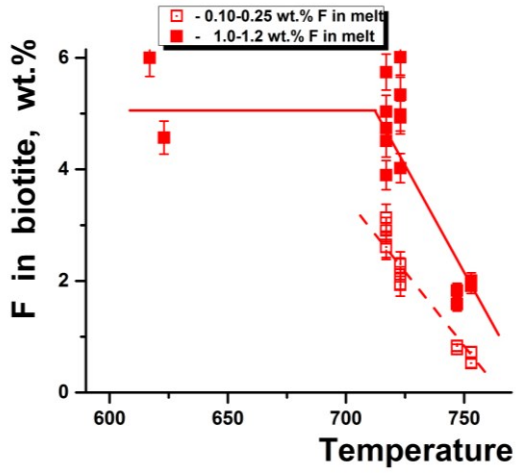


**Fig. 1.** Biotites crystallizing from granite melt in experiments.

**Fig. 2.** Fluorine content in synthesized biotite depending on changes in temperature and fluorine content in the melt.

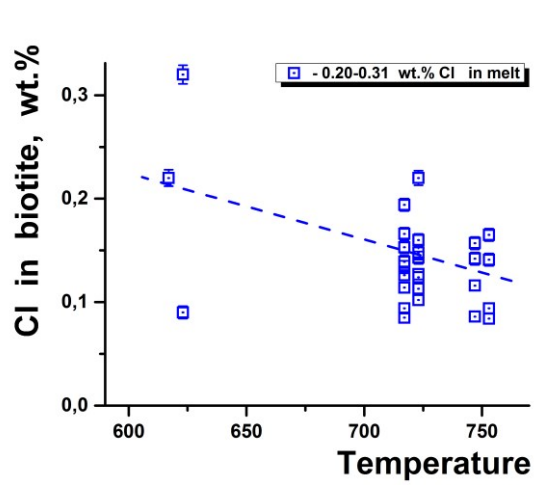


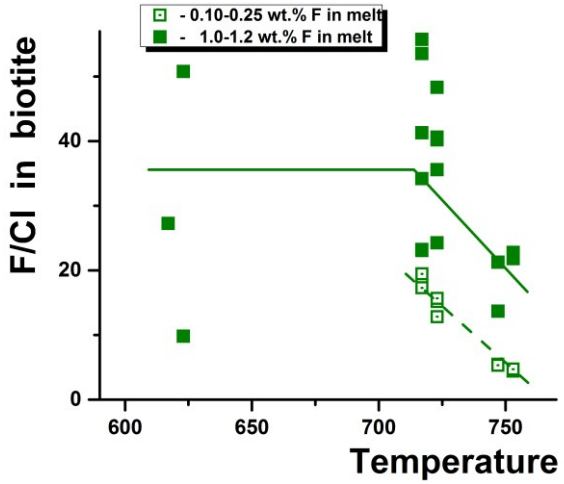


**Fig. 3.** Chlorine content in synthesized biotite depending on temperature changes.

**Fig. 4.** F/Cl ratio in synthesized biotite as a function of temperature change.

It has been experimentally established that with a relatively small decrease in temperature from 750° to 720°C, the fluorine content in biotite increases several-fold, from 0.5–0.8 wt.% to 1.9–3.1 wt.% at initial solution of 1M HF + 1M HCl, and from 1.6–2.0 wt.% to 3.9–6.0 wt.% at initial solution of 5M HF + 1M HCl (Fig. 2). With a further decrease in temperature to 620°C, the fluorine content in biotite appears to remain constant, although the number of analyses at $T$ = 620°C is clearly insufficient, and these data require further clarification.

The dependence of the chlorine content in biotite on temperature shows (Fig. 3) that with decrease in temperature from 750° to 620°C, the chlorine content slightly increases from 0.08–0.17 wt.% up to 0.09 – 0.32 wt.%.

The dependences of the F/Cl ratios in biotite on temperature (Fig. 4) are similar in shape to the dependences of the F contents in biotite in Fig. 2. Thus, with decrease in temperature from 750° to 720°C, the F/Cl ratio in biotite increases by 3–4 times at the initial 1M HF + 1M HCl solution (from 4.4–5.5 to 12.8–23.0) and by approximately two times at the initial 5M HF + 1M HCl solution (from 13.7–22.8 to 23.2–55.8). With further decrease in temperature to 620°C, the F/Cl ratio in biotite does not change.

The fluorine partition coefficient between biotite and melt at the initial 5M HF + 1M HCl solution remains virtually unchanged with decreasing temperature from 750°C to 620°C, varying in the range of 3.9–6.5. At lower HF contents (initial 1M HF + 1M HCl solution), it increases significantly from 7.5–11.1 to 11.5–16.5 in the temperature range of 750–720°C (Fig. 5).

The chlorine partition coefficient between biotite and melt remains virtually constant with changing temperature, varying in the range of 0.39–0.92 (Fig. 6).

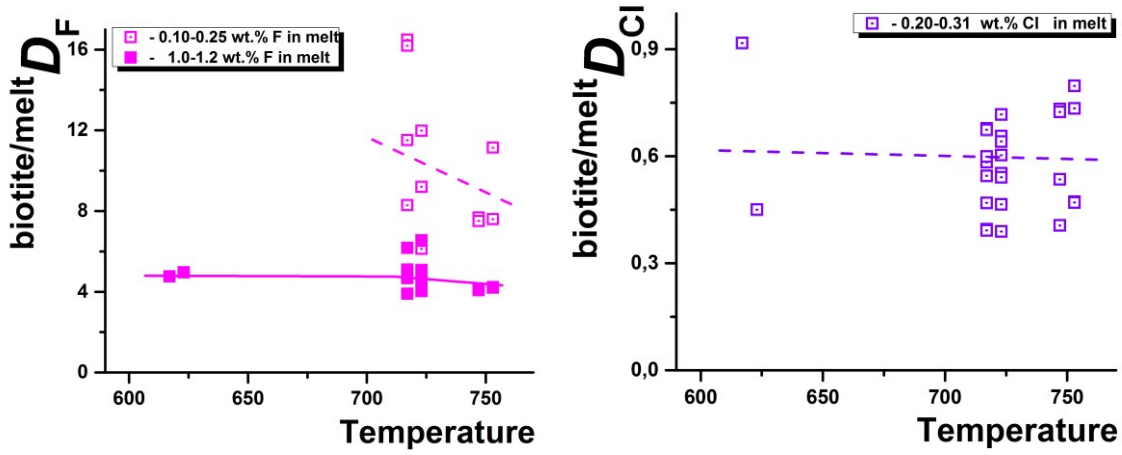


**Fig. 5.** Partition coefficient of fluorine between synthesized biotite and granite melt depending on the change in temperature and fluorine content in the melt.

**Fig. 6.** Partition coefficient of chlorine between synthesized biotite and granite melt depending on temperature changes.

**Table 4.** Chemical composition of natural biotites 1 from granites of the Khangilai massif

| Compo-nents | n [1] | $SiO_2$ | $TiO_2$ | $Al_2O_3$ | $FeO_{tot}$ | MnO | MgO | $K_2O$ | F [2] | Cl [2] | Total | F/Cl [2] | $D_F^{Bt/ml}$ [3] | Mg# [4] |
|---|---|---|---|---|---|---|---|---|---|---|---|---|---|---|
| Biotite 1 | 10 | 38.1 | 3.4 | 17.4 | 24.2 | 0.3 | 5.6 | 9.7 | 1.07-1.77 / 1.39 | 0.02-0.07 / 0.05 | 100.1 | 22-34/ 27 | 10.7-17.7 / 13.9 | 43 |

[1] Number of analyses. [2] Ranges of F, Cl, and F/Cl ratio contents and their average values. [3] Fluorine partition coefficients between biotite and granite melt. [4] $Mg^{\#}$ value of biotite, equal to the 100×Mg/(Mg+Mn+Fe) mole ratio.

**Comparison of the compositions of synthesized and natural biotites.** Synthesized biotites show lower FeO (7.5–13.6 wt.%) and $TiO_2$ (1.3–2.4 wt.%) contents compared to natural micas (24.2 wt.% FeO and 3.4 wt.% $TiO_2$) (Tables 2 and 4), which is likely due to the interaction of these metals with the platinum of the capsule walls during high-temperature experiments (iron can significantly dissolve in platinum, and titanium forms intermetallic compounds with platinum).

***Funding.*** *This study is fulfilled under financial support of the project of the Ministry of Education and Science of Russia, project No. 13.1902.24.44, agreement No. 075-15-2024-641.*

## Gorbachev P.N., Nekrasov A.N., Gorbachev N.S. Experimental modeling of contamination of sulfate-bearing marls in basalts of the mokulaevo formation (Norilsk). *UDC 550.4*

Korzhinskii Institute of Experimental Mineralogy RAS
Chernogolovka, Chernogolovka, Moscow district, Russia
p_gor@mail.ru

**Abstract.** This paper presents the results of an experimental study of the interaction of basaltic melts from the Mokulaevo Formation (Norilsk) with host rocks (sulfate-bearing marls) of the Siberian Platform platform cover. The experiments were conducted at P = 1 atm and T = 1250°C in alundum crucibles using a crucible-in-crucible experimental setup with a powder ($Al_2O_3$) seal. The experimental results showed that some runs exhibited anomalous Cu behavior: a) lower Cu distribution coefficients in the sulfide melt relative to its content in the silicate phase; b) higher Cu content in the silicate melt than in the sulfide melt.

***Keywords****: experiment; basalt; sulfide melt; Norilsk; contamination; buffer; oxygen fugacity*

**Study and analysis of the original samples**. Basalt samples from the Mokulaevskaya Formation (mk) in the Norilsk region were used as the initial composition. The following compositions were used (wt.%): $SiO_2$ – 47.65, $TiO_2$ – 1.26, $Al_2O_3$ – 15.31, FeO – 12.92, MgO – 7.30, CaO – 10.72, $Na_2O$ – 2.09, $K_2O$ – 0.38, $SO_3$ – 0.02. The following platform cover host rock samples were used: red-brown marl, greenish-gray marl with anhydride interlayers, and greenish-gray marl with anhydride and rock salt interlayers (Table 1). All samples were provided by V. A. Radko (Norilskgeologiya).

**Table 1.** Average composition of host rocks of the platform cover of the Norilsk region (wt.%): 1 - greenish-gray marl with anhydrite interlayers (formation D1); 2 - greenish-gray marl with anhydrite and rock salt interlayers (formation D1); 3 - red-brown marl (formation D2).

| № | $SiO_2$ | $TiO_2$ | $Al_2O_3$ | FeO | MgO | CaO | $Na_2O$ | $K_2O$ | $SO_3$ |
|---|---|---|---|---|---|---|---|---|---|
| 1 | 29.67 | 0.68 | 10.75 | 5.72 | 13.6 | 30.16 | 0.52 | 0.88 | 7.21 |
| 2 | 28.86 | 0.33 | 4.89 | 2.08 | 2.92 | 23.11 | 0.12 | 2.76 | 34.43 |
| 3 | 30.16 | 0.45 | 9.31 | 5.14 | 20.99 | 31.23 | 0.96 | 1.12 | 0.04 |

**Preparation and setup of experimental ensembles.** Tablets (10 x 15 mm in size) were cut from the host rock samples and then pierced in a drying oven at 150°C to remove residual water. Powdered basalt was also calcined at the same temperature. The powdered basalt was poured into alundum crucibles, into which a piece of the host rock was then inserted. An $fO_2$ buffer mixture was prepared by mixing weighed portions of its components in the required ratio.

**Experimental technique.** The experiments were conducted at P = 1 atm and T = 1250°C in alundum crucibles in KAO-40 high-temperature furnaces using a crucible-in-crucible experimental assembly with a powder ($Al_2O_3$) seal. The furnace temperature was regulated and controlled using a Minitherm 300.31 microprocessor controller and was maintained at ±0.1°C. Oxygen fugacity was controlled using a $BaCO_3$ + BaO + C + FeO + $Fe_3O_4$ buffer mixture. Some experiments lasted 2, 3.5, and 5 hours, respectively. The $BaCO_3$-BaO-C-FeO-$Fe_3O_4$ $fO_2$ buffer mixture was prepared by mixing weighed portions of its components (pure and special purity grades) in the required ratio.

The experiments were conducted using the quenching method. After holding for the required number of hours, the crucibles were removed from the hot zone of the furnace and exposed to air. The crucibles containing the samples were then sawn lengthwise, polished, and prepared for further examination with a microprobe.

Analytical studies were conducted using two types of digital scanning microscopes:

1). TESCAN VEGA TS-5130 MM with the INCO ENERGY 350 energy-dispersive spectrometer analytical attachment with an INCO M PENTA FEX FET 3 semiconductor Si (Li) detector;

2). TESCAN VEGA II XMU with the INCO ENERGY 450 energy-dispersive spectrometer analytical attachment with an INCA X-SIGT and INCA WAVE 700 semiconductor Si (Li) detector.

**Experimental results.** The results of experiments studying the interaction of basaltic melt with red-brown marl at T = 1250°C for 3.5 hours are shown in Fig. 1.

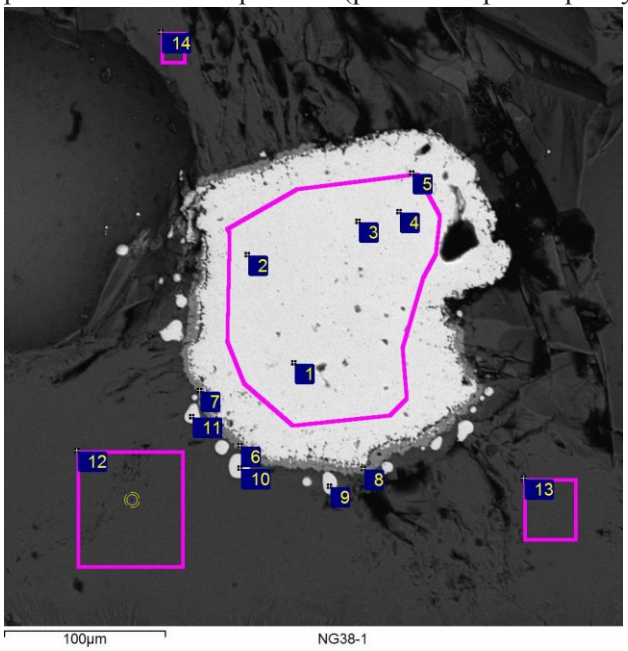


**Fig. 1.** Micrographs of the quenched sample after the experiment. T = 1250°C, t = 3.5 hours.

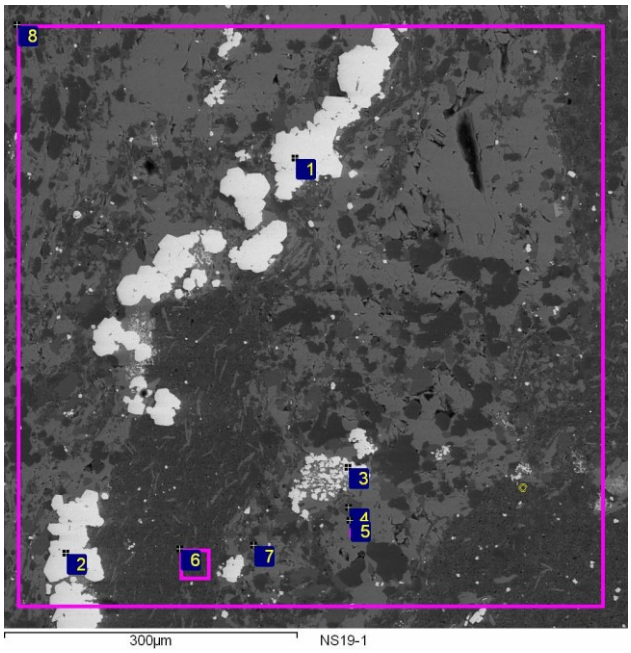


**Fig. 2.** Micrographs of the quenched sample after the experiment. T = 1250°C, t = 3.5 hours. Formation of sulfide melt during xenolith dissolution.

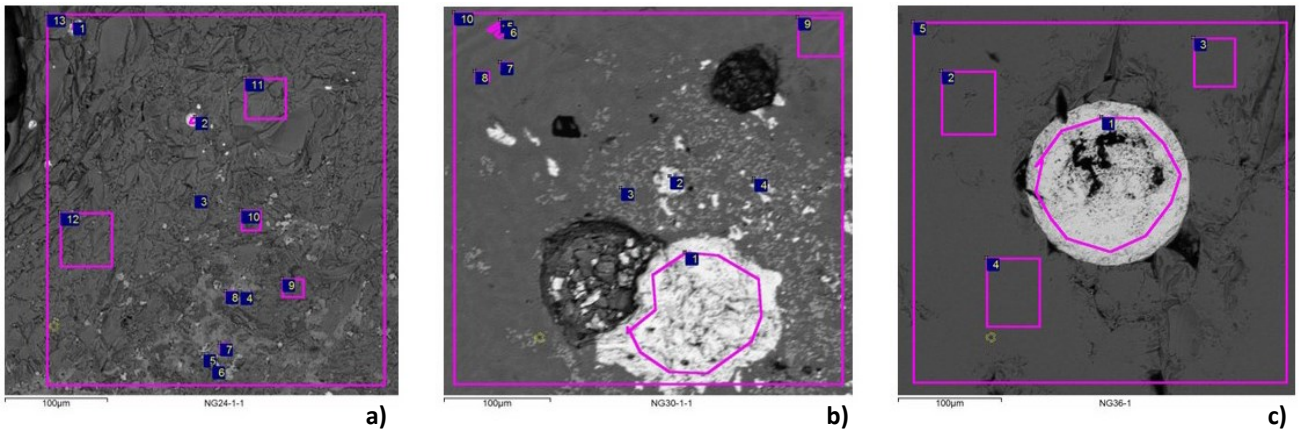


**Fig. 3.** Micrographs of a quenched sample after an experiment at T = 1250°C and an experiment duration of 2 hours (a), 3.5 hours (b), and 5 hours (c), respectively. Formation of a sulfide melt during xenolith dissolution**.**

When basalt was contaminated with xenolith during melting, the basaltic melt interacted with the xenolith and dissolved it, resulting in the formation of an assemblage in the basaltic melt (Fig. 1): chromium-spinel (points 1-5), chromite (points 6-8), Fe-metal (points 9-11), and silicate matrix (points 12-14). In the chromite-Fe-metallic phase assemblage, Cu and Ni have a higher affinity for the metallic phase. The distribution coefficients $K_D$ of the copper content in chromite relative to the iron phase are $K_D^{Cu} = C_{Cu}^{Crt} / C_{Cu}^{Fe\text{-}met} = 0.61$, $K_D^{Ni} = 0.063$, $K_D^{Fe} = 0.161$, respectively. The copper distribution coefficients $K_D$ for chromite relative to its content in the silicate phase, $K_D^{Cu} = C_{Cu}^{Crt} / C_{Cu}^{sil} = 1.6$ and $K_D^{Fe} = 1.287$, respectively.

The results of experiments studying the interaction of basaltic melt with greenish-gray marl interlayered with anhydrite at T = 1250°C for 3.5 hours are shown in Fig. 2.

The silicate portion of the quenched sample is $Na_{0.03}Mg_{0.62}Al_{3.1}Si_{8.8}K_{2.6}Ca_{0.03}Fe_{0.4}O_{24}$; the sulfide portion is $Fe_{31}S_{64}$, with an Fe-S ratio close to that of pyrite.

In the silicate melt-sulfide melt association, anomalous copper behavior is observed; its content in the silicate melt is higher than in the sulfide melt. The copper distribution coefficients $K_D$ in the sulfide melt relative to its content in the silicate phase, $K_D^{Cu} = C_{Cu}^{MeS} / C_{Cu}^{sil}$ are 0.125, $K_D^{Ni} = 1.1$, $K_D^{Fe} = 19.5$ respectively.

The results of experiments on the interaction of basaltic melt with greenish-gray marl with anhydrite + rock salt interlayers at T = 1250°C, t = 2, 3.5 and 5 hours, respectively, are shown in Fig. 3 (a, b, c). With an experiment duration of 2 hours, heterogeneity is observed in the quenched sample; the silicate matrix (analysis points 9-13, Fig. 3a) contains inclusions of Na (points 7, 8) and K (points 4-6) chlorides, and Fe-sulfide melt (points 1-3).

In the quenched sample, anomalous copper behavior is observed; its content in the silicate melt is higher than in the sulfide melt. The copper distribution coefficients $K_D$ in the sulfide melt relative to its content in the silicate phase $K_D^{Cu} = C_{Cu}^{MeS} / C_{Cu}^{sil}$ are 0.546, $K_D^{Ni} = 13.6$, and $K_D^{Fe} = 4.65$, respectively.

In the experimental sample with a duration of 3.5 hours, standard copper behavior is observed; chalcophile properties are observed in the sulfide-silicate melt association, and Cu is concentrated in the sulfide melt. The $K_D$ distribution coefficients for copper content in the sulfide melt relative to its content in the silicate phase, $K_D^{Cu} = C_{Cu}^{MeS} / C_{Cu}^{sil}$ are 9. However, the $K_D$ value is significantly lower than under standard conditions.

Melting basalt for 5 hours maintains a relatively homogeneous composition. The silicate matrix contains inclusions of sulfide globules formed during sulfide saturation of the silicate melt with sulfur from the xenolith during its dissolution in the basaltic melt.

The $K_D$ distribution coefficients for nickel content in the sulfide melt relative to its content in the silicate phase, $K_D^{Ni} = C_{Ni}^{MeS} / C_{Ni}^{sil}$ are 115 and $K_D^{Fe} = 4.11$, respectively, which is consistent with the Ni distribution under standard conditions.

Heterogeneity is observed in the quenched sample, which inherits the heterogeneity of the original sample and the products of the interaction of the basaltic melt with the xenolith. In the quenched sample, the silicate matrix (points 9-13) contains inclusions of Na chlorides (points 7, 8) and K chlorides (points 4-6), and Fe-sulfide melt (points 1-3).

*This work was carried out as part of Russian Science Foundation project No. 25-47-00051.*

## Kazakova A.A.[1], Shchekina T.I.[2] Cryolite as an indicator of rare metal mineralization from the standpoint of experimental data in a granite system with fluorine. *UDC 552.11*

[1]Vernadsky Institute of Geochemistry and analytical chemistry RAS (GEOKHI RAS), Russia, 119991, Moscow, st. Kosygina, 19, aleks7975@yandex.ru,
[2]Lomonosov Moscow State University, Department of Geology, Russia, 119991, Moscow, st. Leninskiye gory, 1, t-shchekina@mail.ru,.

**Abstract.** A study of a water-silicate-salt granite system at T = 500–700°C and P = 1 kbar under fluorine-saturated conditions and involving rare elements was conducted. Experiments were conducted in a model granite system using a high-pressure gas facility at the IEM RAS. A silicate-salt mixture of the following reagents was used as starting compositions: dried $SiO_2$ gel, LiF, $K_2SiF_6$, NaF, $AlF_3$, $Al_2SiO_5$, and $Al_2O_3$. The ratios were selected such that the expected silicate melt composition in the experimental products was close to that of cryolite-containing granites. The experiments were carried out according to the following scheme: the silicate-salt mixture was heated to a temperature of 800°C at 1 kbar with 10 wt. % $H_2O$, held for 3 days, then slowly cooled to a given temperature of 500, 600 or 700°C and held for 3 days. At 800°C, the melt was stratified into two liquids in the experiments: silicate and salt. The following phases were reproduced in all the experiments: L+LF+Crl+FP+Fl (700°C); L+LF+Qz+Crl+Pln+FP+Fl (500-600°C), where L is a silicate melt, LF is a salt melt, Qz is quartz, Crl is cryolite, Pln is polylithionite, FP are quenching fluorine-containing phases, and Fl is an aqueous fluid. The entire REE series (Ln, Sc, Y) was added to all experiments. Fluorine plays a key role in the acid-base processes occurring in the system, acting as a strong oxidizer and forming stable complexes with alkaline elements (Li, Na, K) and Al, which form a salt melt, and with a decrease in temperature, cryolite ($Na_3AlF_6$) and cryolithionite ($Na_3Al_2(LiF_4)_3$) crystallize. With a decrease in temperature from 700 to 600-500°C, a rim of Li-F mica (polylithionite) forms at the contact of the salt melt with the aluminosilicate. Rare earth elements were distributed predominantly in favor of the salt-like cryolite phase by bulk content and formed their own mineral phases in the form of $LnF_3$ complexes with a decrease in temperature from 700 to 500°C. Thus, in our system, the accumulator of fluorine (a mineralizing element) is cryolite, and to a lesser extent mica. REE fluorides often crystallize in paragenesis with these elements, similar to what is observed at rare-metal deposits. Experimental results support the assertion, based on geological observations, that the presence of cryolite in granites should be considered an indicator of rare-metal-rare-earth mineralization.

***Keywords***: *cryolite; silicate melt; salt melt; aqueous fluid; rare earth elements; immiscibility; fluoride phases; fluorine activity*

**Introduction.** One of the causes of liquation in silicate melts is the difference in the ordering of long-range and short-range elements. For example, weak sodium and potassium cations are displaced by strong silicon and aluminum cations, giving rise to repulsive forces between melt groupings and between network-forming alkali metal cations (Kompanichenko, 1982). The formation of cation-anion associations leads to microheterogeneity in the melt, and a strong shift in equilibrium toward a combination of certain cations and anions can, under certain conditions, lead to significant ion rearrangement and cause macroheterogeneity, i.e., the formation of two immiscible phases.

In the model granite system Si-Al-Na-K-Li-F-O-H studied here, in addition to short-range cations, volatile components, fluorine and water, as well as lithium, are present. Volatile components lower the melting point and reduce the melt viscosity. In acidic melts, strong homopolar ≡Si-O-Si≡ bonds are destroyed due to viscosity. Increasing the modifying oxide content leads to the replacement of some ≡Si-O-Si≡ bonds with heteropolar ≡Si-O-M bonds (Kogarko, Krigman, 1981). According to IR spectroscopy data, the addition of fluorine to glasses leads to depolymerization of silicon-oxygen tetrahedra, forming ≡Si-F bonds. It has also been suggested that fluorine may be bound to modifying cations, forming M-F bonds (Kogarko, Krigman, 1981). An alkali-aluminofluoride melt, in equilibrium with an aluminosilicate melt and close in composition to cryolite, existed only in a narrow high-alumina region (Gramenitskiy et al., 2005; Alferyeva et al., 2011), and in the plumasite system, upon cooling at 7 mol.% fluorine, the growth of silicate-salt immiscibility ceases, and villiaumite crystals begin to precipitate (Kogarko, Krigman, 1981). With an increase in the fluorine content above 3 wt. % in the model granite system studied by the authors, K-Na cryolite consistently appeared at the liquidus.

Lithium expands the boundaries of immiscibility fields. The introduction of Li (1,5 wt.%) into the system led to a significant expansion of the salt melt field in the system due to a decrease in the cryolite field (Alferyeva et al., 2011). This is explained by the "theory of mutual salt systems, according to which the dimensions of the immiscibility fields correlate with the values of the free energies of exchange reactions between the melt components of the type: AX + BY = AY + BX, where A and B are cations, and X and Y are anions. Consequently, the free energy of exchange reactions between the components of a silicate-salt melt is very large in absolute value, which is associated with the presence of wide liquation regions in these melts" (Kogarko, Krigman, 1981). A large region of immiscibility in the Si-Al-Na-(K)-Li-F-O-H system has been delineated in (Gramenitskiy et al., 2005; Shchekina et al., 2020; Rusak et al., 2024).

The difference in electrostatic interactions between melt ions is the primary cause of immiscibility. Immiscibility in fluoride-silicate melts

indicates that fluorine in the melt is associated with modifier cations and does not depolymerize the silicon-oxygen matrix of the melt (Kogarko, Krigman, 1981).

Salt and aluminofluoride melts are of particular importance in explaining the distribution pattern of rare earth elements during the differentiation of granite magmas and subsequent metasomatism and ore formation in granites (Irber, 1999; Gusev, Gusev, 2011). Lithium plays a special role in influencing the distribution of rare earth elements in favor of salt melts (Gramenitskiy, Shchekina, 2005; Veksler, 2005; Shchekina et al., 2020, 2021). Thermodynamic parameters also affect their behavior: the higher the pressure at 700 and 800°C, the lower the partition coefficients between salt and aluminosilicate melts (Shchekina et al., 2020, Rusak et al., 2024).

**The purpose and objectives of the study.** The aim of this study was to investigate the role of fluoride melts as rare earth element concentrators and their complexes formed during experiments in the model granite system Si-Al-Na-K-Li-F-O-H. To achieve this goal, the following tasks were completed: setting up experiments at 500-800°C and 1 kbar, a detailed study of the rare earth phases, and their interpretation.

**Methodology.** For the experiments, the initial composition of the aluminosilicate melt was chosen, close in composition to the granite eutectic quartz-albite-orthoclase at 690°C, 1 kbar $H_2O$, 1 wt. % F (Manning, 1981), and containing 1,5 wt. % Li. The ratio of the atomic quantities of the main elements was Si:Al:(Na+K+Li) = 70:15:15. The alkali element ratio was Na:K:Li = 7.5:2.5:5. An aluminofluoride component (corresponding by stoichiometry to the compound $(Na,K,Li)_3AlF_6$) was added to the silicate composition in an amount sufficient to saturate the aluminosilicate melt and separate the isolated aluminofluoride phase). The water content in the system ranged from 0 to 50 wt. %. Dried $SiO_2$ gel, NaF, LiF, $AlF_3$, $Al_2O_3$, $K_2SiF_6$ were used as initial reagents. Rare earth elements, as well as Sc and Y at 700 and 800°C were introduced into the system in the form of oxides in an amount of 0,5 wt. % of the element. In the experiments at 500-600°C, REE were introduced in specific pairs to avoid line overlap on the device: $Y_2O_3$, $La_2O_3$; $Sm_2O_3$, $Gd_2O_3$, $Tb_2O_3$; $CeO_2$, $Eu_2O_3$ and $Ho_2O_3$; $Dy_2O_3$; $Pr_2O_3$, $Lu_2O_3$, $Sc_2O_3$; $Er_2O_3$, $Yb_2O_3$; $Nd_2O_3$, $Tm_2O_3$; $Sc_2O_3$, $Gd_2O_3$. A more detailed description of the operating procedure is given in the articles (Shchekina et al., 2020; Rusak et al., 2024). The experiments were carried out on a high-pressure gas setup with internal heating at a temperature of 500-800°C and a pressure of 1 kbar at the Korzhinsky Institute of Experimental Mineralogy of the Russian Academy of Sciences. The experiments were conducted using the following scheme: the silicate-salt mixture was heated to 800°C at 1 kbar, held for 3 days, then slowly cooled to the target temperature of 500 and 600°C and held for 3 days. Experiments at 700-800°C and 1 kbar were conducted using the standard scheme without stepwise temperature changes. The temperature measurement error was ±5°C, and the pressure measurement error was ±10 bar. Oxygen fugacity corresponded to the NNO buffer. The quenching rate was 150-200 degrees per minute. The duration of the experiments was 6-7 days. The study of the structure of the samples, the morphology of the phases and the chemical composition was carried out using a Jeol JSM-IT500 scanning electron microscope (Jeol, Japan) with an Oxford X-MaxN energy-dispersive spectrometer (Oxford Instrument Ltd., UK) and a Superprobe JXA-8230 electron probe microanalyzer (Jeol, Japan) in the laboratory of local methods for studying matter at the Department of Petrology and Volcanology of the Geological Faculty of Moscow State University.

**Results of the study.** At 800°C, the melt in the experiments separated into two liquids: silicate and salt. The following phases were reproduced in all experiments: L+LF+Crl+FP+Fl (700°C); L+LF+Qz+Crl+Pln+FP+Fl (500-600°C), where L is an aluminosilicate melt, LF is a salt melt, Qz is quartz, Crl is cryolite, Pln is polylithionite, FP is quenching fluorine-containing phases, and Fl is an aqueous fluid. As the temperature decreased from 700 to 600-500°C, a rim of LiF mica (polylithionite) formed at the contact between the salt melt and the aluminosilicate melt. Rare earth elements were distributed predominantly in favor of the cryolite-like phase, which was salt-like in terms of bulk content, and formed their own mineral phases as the temperature decreased from 700 to 500°C. $MeLnF_4$ and $Me_3LnF_6$ compounds may be formed, and REEs can also form $REEF_3$ compounds. Lithium with heavy REEs can also form compounds with fluorine $LiLnF_4$, for example, Gd, Ho, Tm, and Lu (Batsanova, 1971). The composition of the residual salt melt (LFres) at 600°C contains less aluminum, fluorine, and alkalis, compared to higher-temperature experiments (Shchekina et al., 2020; Rusak et al., 2024, 2025), because most of it is concentrated in newly formed mineral phases - cryolite, polylithionite, and other minerals. The residual salt melt accumulates REEs. In experiments carried out at 600°C, the content of Ce was ~ 8 wt. %, Eu ~ 18 wt.%, Ho ~ 11 wt. %, Sc ~ 24 wt. %, Gd ~ 6,5 wt. % (Table 1).

**Table 1.** Average compositions of residual salt melt for experiments 869 and 874, carried out at 600°C and 1 kbar.

| № exp. | Phases | Si | Al | Na | K | Mg | Ca | F | O | Ce | Eu | Ho | Total |
|---|---|---|---|---|---|---|---|---|---|---|---|---|---|
| 869 | $LF_{res}$ by S | 0,17 | 3,92 | 4,50 | 2,55 | - | 0,56 | 37,15 | 1,93 | 7,71 | 18,22 | 10,86 | 88,94 |
| № exp. | Phases | Si | Al | Na | K | Mg | Ca | F | O | Sc | Gd | | Total |
| 874 | $LF_{res}$ by S | 0,43 | 0,83 | 5,76 | 6,07 | 1,13 | 0,26 | 44,98 | 4,98 | 23,67 | 6,51 | | 94,62 |

Notes. Contents are presented as wt. % of the element.

Fluorides of rare earth elements often gravitate towards the marginal zones of salt globules (Fig. 1 – white Nd and Tm fluorides in BSE).

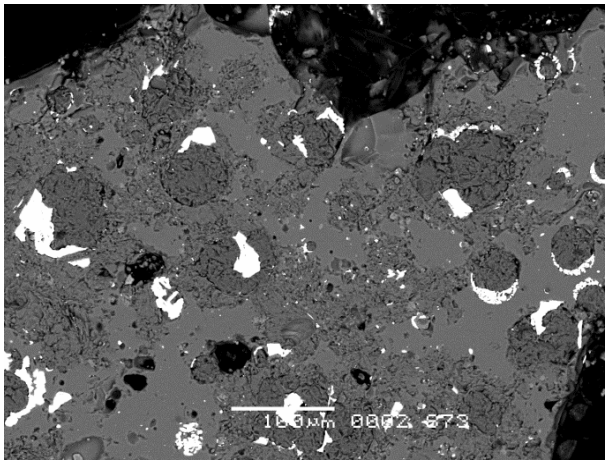

**Fig. 1.** Quenched salt globules immersed in aluminosilicate glass. Neodymium and thulium fluorides are white in BSE. Experimental conditions: T = 600°C, P = 1 kbar, $CH_2O$ = 15 wt. %.

**Conclusions.** In the model granitic agpaitic system Si-Al-Na-K-Li-F-O-H, at high temperatures, the accumulator of fluorine (a mineralizing element) and rare elements is a lithium-containing alkali-aluminofluoride melt, from which cryolite crystallizes at 700°C and 1 kbar, in paragenesis with REE fluorides. Polylithionite, quartz, and feldspars are formed from the fluorine-saturated aluminosilicate melt, similar to what is observed at rare-metal deposits such as Katuginskoye (Rusak et al., 2025) and Zashikhinskoye (Kazakova, Shchekina, 2026 (in press)). A significant expansion of the liquation region in the silicate-salt fluorine-containing model granite system occurs with the addition of lithium.

**Funding sources**. The work was carried out within the framework of the state assignment of the GEOKHI RAS and on the state budget theme "Regimes of petrogenesis of the Earth's internal geospheres" of the Geological Faculty of the Lomonosov Moscow State University.

**References**

Alferyeva Ya.O., Gramenitskiy E.N., Shchekina T.I. Experimental study of phase relationships in a lithium-bearing fluorine-rich haplogranite and nepheline-syenite system // Geochemistry. - 2011. - №. 7. - P. 713-728. [in Russian]

Batsanova L.R. Fluorides of rare earth elements // Uspekhi Chem. - 1971. - Vol. 40. - №. 6. - P. 945-979. [in Russian]

Gramenitskiy E.N., Shchekina T.I., Devyatova V.N. Phase relationships in fluorine-bearing granite and nepheline-syenite systems and element distribution between phases (experimental study). Moscow: GEOS. - 2005. - 188 p. [in Russian]

Gramenitskiy E.N., Shchekina T.I. Behavior of Rare Earth Elements and Yttrium at the Final Stages of Fluorine-Bearing Magma Differentiation // Geochemistry. - 2005. - №. 1. - P. 45-59. [in Russian]

Gusev A.I., Gusev A.A. Tetrad Effect of Rare Earth Element Fractionation and Its Application in Solving Granitoid Petrology Problems // Advances in Modern Natural Science. - 2011. - № 5. - P. 45-49. [in Russian]

Kazakova A.A., Shchekina T.I. Parageneses of Cryolite-Bearing Granites of the Zashikhinsky Deposit and Their Comparison with Experimental Data in a Model Granite System // Proceedings of the Fersman Scientific Session of the Geological Institute of the Kola Science Center of the Russian Academy of Sciences. - 2026 (in press). [in Russian]

Kogarko L.N., Krigman L.D. Fluorine in Silicate Melts and Magmas. Moscow: Nauka. – 1981. - 126 p. [in Russian]

Kompanichenko, V.N. Liquation Hypothesis of the Evolution of Magmatic Series. Preprint. Vladivostok: Institute of Tectonics and Geophysics, Far Eastern Scientific Center, USSR Academy of Sciences. – 1982. - 44 p. [in Russian]

Rusak, A.A., Shchekina, T.I., Zinovieva, N.G. Cryolite Formation in Granites of the Katuginskoye Deposit from the Perspective of Experimental Results in a Fluorine-Lithium-Containing Granite System // Petrology. - 2025. - Vol. 33. № 5. P. 40–57. [in Russian]

Rusak A.A., Shchekina T.I., Zinovieva N.G., Bychkov A.Yu., Lukanin O.A. Cryolite as a reference mineral of rare-metal mineralization (experimental study) //

Geochemistry. - 2024. - Vol. 69. № 7. - P. 579–595. [in Russian]
Shchekina T.I., Rusak A.A., Alferyeva Ya.O., Gramenitskiy E.N., Kotelnikov A.R., Zinovieva N.G., Bychkov A.Yu., Bychkova Ya.V., Khvostikov V.A. Distribution of REE, Y, Sc, and Li between aluminosilicate and aluminofluoride melts in a model granite system depending on pressure and water content. Geochemistry. - 2020. - Vol. 65. № 4. - P. 343–361. [in Russian]
Shchekina T.I., Rusak A.A., Alferyeva Ya.O., Gramenitskiy E.N., Khvostikov V.A., Kotelnikov A.R., Bychkov A.Yu., Zinovieva N.G. Behavior of lithium in the liquidus part of a high-fluorine granite system at pressures from 10 to 50 MPa. Bulletin of Moscow University. Series 4: Geology. – 2021. № 3. - P. 76–88. [in Russian]
Irber W. The lanthanide tetrad effect and its correlation with K/Rb, Eu/Eu*, Sr/Eu, Y/Ho, and Zr/Hf of evolving peraluminous granite suites. // Geochim. Cosmochim. Acta. - 1999. - V. 63. - № 3/4. P. 489–508.
Manning D. The effect of Fluorine on liquidus phase relationships in the system Qz-Ab-Or with excess water at 1 kb // Contrib. Mineral. Petr. - 1981. - V. 76. - P. 206-215.
Veksler I.V., Dorfman A.M., Kamenetcky M., Dulskii P., Dingwell D.B. Partitioning of lanthanides and Y between immiscible silicate and fluoride melts, fluorite and cryolite and the origin of the lanthanide tetrad effect in igneous rocks. //Geochim. Cosmochim. Acta. 2005. - V. 69. - № 11. - P. 2847–2860.

## Khodorevskaya L.I., Safonov O.G., Spivak A.V., Tushkanova S.A., Nekrasov A.N. Experimental study on melting of graphite-bearing garnet – two mica schist at 500 MPa and 750-800 °C: toward internal sources of $CO_2$ in the Earth's crust. *UDC 552.13*

D.S. Korzhinskii Institute of Experimental Mineralogy of Russian Academy of Sciences (IEM RAS), Chernogolovka Moscow district. khodorevskaya@mail.ru

**Abstract** This work is a continuation of the studies presented in (Safonov et al., 2025). Its objective was to study the possibility of $CO_2$ generation due to graphite-bearing metapelites in the temperature range of 750-800 °C and a pressure of 500 MPa, realized under crustal conditions. The experimental results showed that the onset of metapelite melting is observed at a temperature of approximately 800 °C. Melt formation occurs due to muscovite melting and depends on the concentration of graphite in the system. At low contents (0-6 wt. % graphite), the resulting melts correspond to high-alumina alkali-calcic S-granites. When the graphite content in the original rock exceeded 6 wt%, no melt was observed after the experiments. The increase in solidus temperature is explained by a decrease in fugacity of $O_2$, associated with an increase in the graphite content. Raman spectroscopy did not reveal the presence of $CO_2$ or carbonate phases in the melt. Thus, experiments have shown that at 800 °C in the early stages of partial melting, the role of graphite-containing metapelites as internal sources of $CO_2$ is insignificant.

***Keywords:*** *metapelites; graphite; granitoid melts; dehydration melting; experiment*

**Introduction** $CO_2$ is formed during the degassing of mantle magmas and is a source external to metamorphic rocks. However, there are also internal sources of $CO_2$ associated with the initial presence of carbonate minerals and/or graphite in the protolith (Holloway, 1976; Lowenstern, 2001; Hollister, 1988; Cesare et al., 2005; Nicoli et al., 2022). The mechanism of $CO_2$ formation in graphite-containing protoliths, widely discussed in the literature (Hollister, 1988; Cesare et al., 2005, 2007; Nicoli et al., 2022; Kadik, Lukanin, 1985; etc.). It is associated with the appearance of $O_2$ formed due to the reduction of $Fe^{3+}$ to $Fe^{2+}$ in micas, or due to the interaction of graphite with $H_2O$. There is very limited experimental data confirming or refuting this mechanism. Thus, London et al. (2012) noted the appearance of $CO_2$ as a result of graphite oxidation during the interaction of granite melt with graphite-bearing muscovite-quartz schist at 750-800°C and 200 MPa. Works by Khodorevskaya et al.(2024) and Safonov et al. (2025) present the results of an experimental study of the partial melting of plagioclase-free garnet-two-mica schist with graphite at 500 MPa and 900°C. It was shown that the interaction of graphite with $O_2$, formed as a result of the $Fe_2O_3 \rightarrow FeO$ transition reactions from decomposing micas, provides the appearance of $CO_2$. It is the predominant component of the free fluid phase and also partially dissolves in the melt as molecular $CO_2$ and $CO_3^{2-}$ complexes with alkali and alkaline earth cations. The migration of thes melts into the upper crustal horizons results is the release of $CO_2$, meaning that under high-temperature metamorphic conditions, graphite-bearing metapelites can serve as an effective internal source of $CO_2$. This work is a continuation of the research presented by Safonov et al. (2025). Its goal was to study the possibility of $CO_2$ generation from graphite-bearing metapelites over a wider temperature range, consistent with crustal conditions. The experimental procedure, analysis of the experimental products, study of the compositions of mineral phases, and Raman spectrascopy studies are described in detail in Safonov et al. (2025).

**Experimental results** In experiments conducted at 750-800 °C, the following phases of the original metapelite are preserved: garnet (Grt), biotite (Bt), ilmenite (Ilm), quartz (Qz), muscovite (Ms), and apatite (Ap). The newly formed phases of experiments at 750 °C are represented by potassium feldspar (Kfs) and cordierite (Crd) with a high

graphite content (Table 1). At 800 °C, the newly formed phases in experiments K1, K3, and K2 are represented by potassium feldspar and numerous tiny, sometimes filamentary, clusters of bright, Fe-bearing spinel (Spl) (Fig. 1a). It was not possible to determine the spinel composition correctly due to its small size. Furthermore, small prisms of newly formed biotite $Bt_2$ (Fig. 1b) are present in these same experiments. like Spl, $Bt_2$ only appears when graphite contents is less than 7-9 wt%.

**Table 1**. Graphite content in the starting mixtures and the phase composition of the run products at 500 MPa and 750-800°C

| Run | T,°C | Graphite content, wt % | Run products |
|---|---|---|---|
| D-3 | 750 | 20 | Qz+ Bt+Ms+Gl+Kfs+Ap+Grt+Ilm+Sil |
| D-5 | 750 | 29 | Qz+ Bt+Ms+Gl?+Kfs+Ap+Grt +Ilm+Crd |
| D-4 | 750 | 37 | Qz+ Bt+Ms+Gl?+Kfs+Ap+Grt+Ilm+Crd |
| K-1 | 800 | 0 | Qz+Bt+Kfs+Ms+Ap+Grt+Ilm+Sil±Gl |
| K-3 | 800 | 2.58 | Qz+Bt+Gl+Kfs+Ap+Grt+Ilm+Sil+Spl |
| K-2 | 800 | 5.56 | Qz+Bt+Kfs+Ap+Grt+Ilm+Sil±Gl |
| D-8 | 800 | 9.2 | Qz+Bt ±Gl+Kfs+Ap+Ms+Grt+Ilm+Sil |
| K-4 | 800 | 10 | Qz+Bt+Ms+Kfs+Ap+Grt+Ilm |
| D-9 | 800 | 13.9 | Qz+Bt+Kfs+Ap+Ms+Grt+Ilm |
| K-5 | 800 | 18,26 | Qz+Bt+Ms+Kfs+Ap+Grt+Ilm |
| D-10 | 800 | 25 | Qz+Bt+Ms+Kfs+Ap+Grt+Ilm |

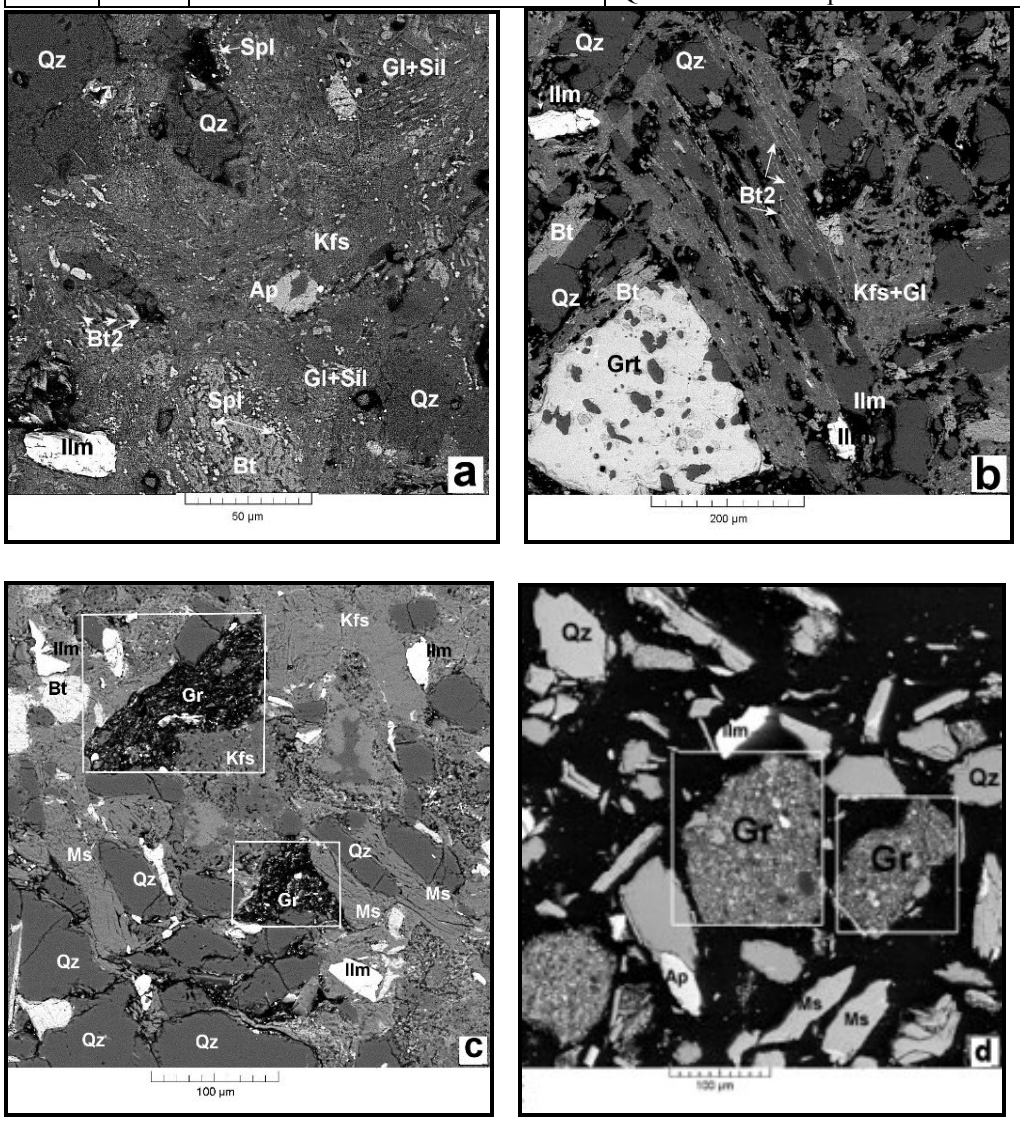


**Fig. 1**. BSE images of the products of the experimental runs. (a-b), bright small crystals of newly formed hercynite-magnetite spinel and $Bt_2$, Gl rims, as well as Gl+Sil areas, quartz, ilmenite (experiments K-1, K-3); (c) - absence of small, bright Spl and $Bt_2$, large crystals of Ms, $Bt_1$, (experiment D-9); (d) - powdery appearance of the sample due to the absence of even a film melt, large micas of Ms, Bt (experiment K-5). Within Fig. 1c-d - graphite with mineral phenocrysts.

In the same samples, Kfs and quenched melt (Gl) outlining Qz grains were observed. The melt, which accounts for a small percentage of the total, contains needle-like sillimanite (Sil) crystals. With an increase in the graphite content in the initial sample above 9 wt% (experiment D-8, Table 1), Fe-containing filamentous phases disappear from the samples; the melt is not visually observed, but it obviously forms as a film, since the minerals after the experiments are cemented together (Fig. 1c). Samples after experiments K-4, D-9 and others, with a high graphite content (Table 1) are a powder with individual, unbound minerals, which indicates the absence of melting (Fig. 1d). Despite the fact that graphite was thoroughly and uniformly mixed with the original rock before the experiments conducted at 750-800 °C, after the experiments its concentration was observed in the form of isolated large, near-round clusters (Fig. 1c, d in the frame).

**Compositions of Crystalline Phases in the Experimental Products.**

After experiments, muscovite contains 10% of the paragonite end-member ($NaAl_2[AlSi_3O_{10}](OH)_2$). The content of the celadonite end-member ($KMgFe^{3+}Si_4O_{10}(OH)_2$) varies, increasing from 10 to 40% with graphite contents from 0 to 25 wt% (Fig. 2).

*Biotite,* both $Bt_1$ and newly formed $Bt_2$, are characterized by similar iron indexes of F = FeO\(FeO+MgO) = 0.60-0.70 at all graphite contents. The Ti content in $Bt_1$ increases slightly compared to the original, from 0.13 to 0.17 f.u. In $Bt_2$ the Ti content reaches 0.30-0.32 f.u., with high-Ti $Bt_2$ appearing only at low graphite contents (< 5.56 wt%) (Fig. 3).

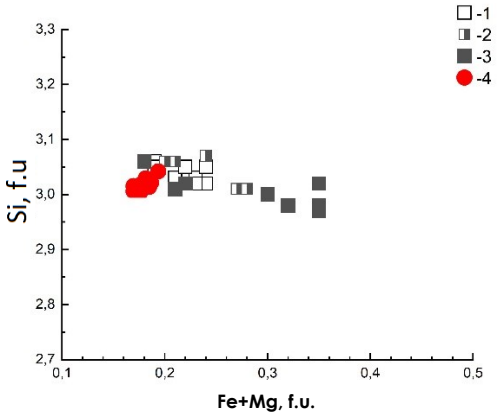


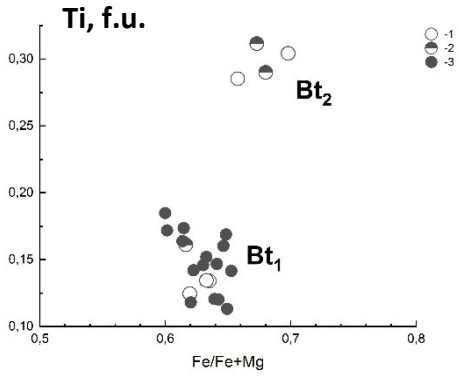


**Fig. 2.** The ratio of Fe+Mg – Si (f. u.) in muscovite: 1-2 – respectively 0-17% graphite, 3 -18-25% graphite, 4- starting Ms

**Fig. 3**. The ratio Fe/(Fe+Mg) – Ti (f. u.) in biotites $Bt_1$ and $Bt_2$: 1 - without graphite, 2 -5.56 wt% graphite, 3 - 10 – 25 wt% graphite

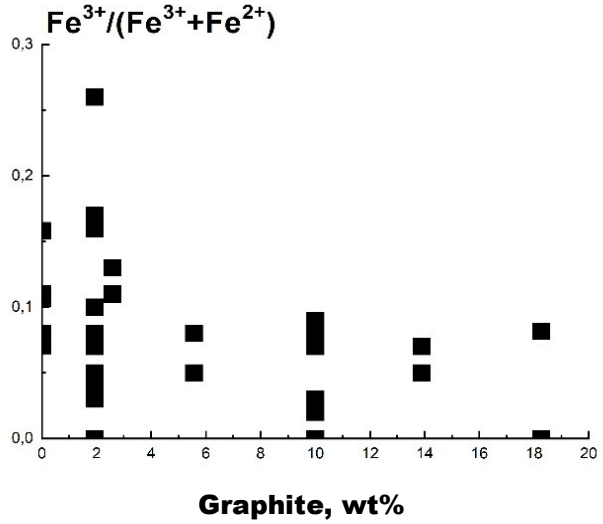


**Fig. 4.** Dependence of the $Fe3^+/(Fe^{3+}+Fe^{2+})$ ratio of the ilmenite on graphite content

*Garnet* in all samples is characterized by a high almandine component of $Grs_{0.05}Alm_{0.95\text{-}1.0}Prp_{0.03}$.

*Ilmenite* The $Fe^{3+}/\Sigma Fe$ ratio in the original ilmenite in schist is ≈ 0.05. After the experiments, this ratio at a low graphite content increases slightly (to 0.12±0.10), then decreases, remaining at approximately a constant level at a graphite content of more than 6 wt% (Fig. 4).

*In potassium feldspar,* the albite content increases from $KAlSi_3O_8$ to $(K_{0.5}Na_{0.5})AlSi_3O_8$ as the graphite concentration increases.

The composition of *cordierite* is expressed by the formula $(Mg_{0.76}Fe_{0.9})[Al_{4.28}Si_{4.6}O_{18}]\cdot nH_2O$, F = 0.48-0.53.

*Melt compositions*. The chemical composition of the quenched melt was determined only in runs K-1 and K-3. The melts correspond to high-alumina alkali-calcic S-granites: A/CNK = 1.40-1.50, A/NK = 1.50-1.60. In the remaining runs, melt was either

absent (runs D-9, K-5, D-10) or very small, so its composition could not be accurately determined.

**Raman Spectroscopy of the Glasses .** Due to the small volumes of the quenched melt, gas inclusions (bubbles) were not observed in any of the samples. The figure 5 shows the Raman spectra of glass from sample K3. The glass exhibits OH groups and peaks D (1444 $cm^{-1}$) and G (1580 $cm^{-1}$) of disordered graphite. The spectrum of the remaining samples is similar. No other peaks related to graphite derivatives were detected.

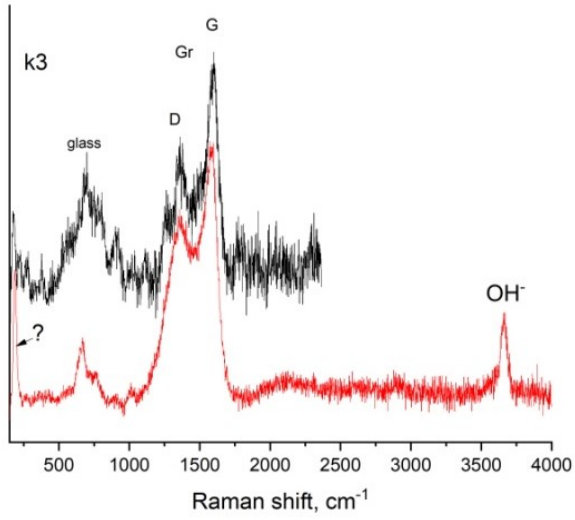


**Fig. 5.** Raman spectra of glass in the products of runs K-3

**Discussion of experimental results**

Experimental results show that schist melting begins at 800°C. The aluminosilicate portion of muscovite is primarily converted into feldspar and the melt, which increases the celadonite content. According to (Mityaev et al., 2022), the melting reaction are controlled by the equilibria: Ms + Qz + Bt1 = Bt2 + Kfs + Sil + Spl + Gl (1). At relatively low graphite contents in the initial sample (less than 6-8 wt%, Table 1), melt rims are visible; at higher graphite contents, only thin covers melts cementing the minerals exist, and at graphite contents ≥ 10 wt%, melting is absent. The absence of melting at high graphite contents may be due to a slowdown in the equilibrium reactions between the phases due to a decrease in the area of their contacts. However, the appearance of isolated graphite clusters in the experimental products suggests that direct contacts between minerals were not disrupted in sample regions free of such clusters. Therefore, it was assumed that a state close to equilibrium could have been achieved in experiments with 7-10-day exposure at 800°C, and that changes in the composition of mineral phases, and the presence or absence of solidus, are associated with varying graphite contents in the system, rather than kinetic factors. Experimental data (Scaillet, Macdonald, 2001, and others) indicate that a decrease in $fO_2$ can increase the solidus temperature. A variable valence of minerals, in particular the Fe3+/Fe2+ ratio in biotite and ilmenite, is an indicator of $fO_2$ changes in the system. Furthermore, in biotite, $Ti^{4+}$ replaces $Al^{3+}$ in the octahedral layer at high $fO_2$. Therefore, with increasing reducing conditions, the Ti4+/(Ti4++AlVl) ratio should decrease. However, according to our experiments, both the Fe3+/(Fe3++Fe2+) ratio and the Ti4+/(Ti4++AlVl) ratio in biotite remain virtually unchanged with increasing graphite concentration. Therefore, Bt cannot serve as an indicator of changes in $fO_2$.

A decrease in the Fe3+/ΣFe ratio in ilmenite or a decrease in the X(Ilm) - X(Hem) ratio indicates that with an increase in the graphite content, the O2 fugacity decreases from lg $fO_2$ = -14.5 to lg $fO_2$ = -16 (Table 2, Buddington, Lindsley, 1964). Thus, the absence of melting in samples D-9, K-5, D-10, i.e., an increase in the solidus temperature, is explained by a decrease in O2 fugacity caused by an increase in the graphite content in the system.

**Table 2.** Ratio of X(Ilm) X(Hem) and lg $f_{O_2}$ in ilmenites after experiments

| Run | Graphite content, wt % | X(Ilm) | X(Hem) | lg $f_{O_2}$ |
|---|---|---|---|---|
| K1 | 0,00 | 0,87 | 0,09 | <-14.5 |
| 7D | 1,93 | 0,89 | 0,08 | <-14.5 |
| K3 | 2,58 | 0,86 | 0,11 | -14 |
| K2 | 5,56 | 0,91 | 0,06 | <-15 |
| K4 | 10,00 | 0,89 | 0,04 | -16 |
| K5 | 18,26 | 0,95 | 0,04 | -16 |

**Conclusions**

1. Experimental results showed that, at high T-P parameters, graphite is completely concentrated from dispersed graphite into graphite clusters with small inclusions of other minerals. The possible formation of graphite ores in the form of ellipsoidal or rounded rods and nests in natural conditions is partly explained by the effect of high parameters in the absence of a fluid phase.

2. Cordierite obtained at 750 °C can serve as an indicator of high (over 20 wt%) graphite contents.

3. At 800°C and 500 MPa, the initial stage of metapelite melting is observed. Melt formation occurs due to muscovite melting and depends on the concentration of graphite in the system. At low graphite contents (0-6 wt%), the resulting melts correspond to high-alumina alkali-calcic S-granites: A/CNK = 1.40-1.50, A/NK = 1.50-1.60. At graphite contents in the original rock exceeding 10 wt%, no melt is observed, and the rock does not melt. The increase in solidus temperature is explained by a

decrease in $O_2$ fugacity associated with an increase in graphite content.

4. Raman spectroscopy did not reveal the presence of $CO_2$ in the melt, which is explained by the very small amount of melt formed. In addition, the component composition of the fluid under graphite saturation conditions at given T-P parameters is represented mainly by $H_2O$ ($X_{H2O}$ = 0.7-0.8), with the content of carbon-containing phases $X_{CO2, CH4, CO}$ <0.3. (Danilov, 2005).

5. Thus, experiments have shown that at 800°C in the early stages of partial melting, the role of graphite-containing metapelites as internal $CO_2$ sources is insignificant. Only metapelites at high temperatures (>900°C) can be effective accumulators and transporters of $CO_2$.

**Funding**. The work was carried out within the framework of the research project of the IEM RAS No. FMUF-2022-0004.

**References**

Cesare B., Meli S., and Nodari L. $Fe^{3+}$ reduction during biotite melting in graphitic metapelites: another origin of $CO_2$ in granulites // Contrib. Mineral. Petrol. 2005. V. 149. P. 129–140.

Cesare, B., Maineri, C., and Toaldo, A.B., Immiscibility between carbonic fluids and granitic melts during crustal anatexis: a fluid and melt inclusion study in the enclaves of the Neogene Volcanic Province of SE Spain // Chem. Geol. 2007. V. 237. P. 433–449.

Hollister, L.S., On the origin of $CO_2$-rich fluid inclusions in migmatites // J. Metamorph. Geol. 1988. V. 6. P. 467- 474.

Holloway J.R. Fluids in evolution of granitic magmas: Consequence of finite $CO_2$ solubility// GSA Bull. 1976. V. 87. P. 1513–1518.

Kadik A.A. and Lukanin O.A. Paths for mantle outgas sing during melting: changes in fluid composition and conditions in basaltic magmas during migration to the surface// Int. Geol. Rev. 1985. V. 27. P. 573–586.

Khodorevskaya L. I., Safonov O. G., Spivak A. V., Kosova S. A. On the Possible Sources of $CO_2$ during High-Temperature Metamorphism in the Continental Crust. I. Experimental Study of Partial Melting of Graphite-Containing Garnet-Two-Mica Schist at 500 MPa and 900 °C // Proceedings of the Fersman Scientific Session of the Geological Institute of the Kola Science Center of the Russian Academy of Sciences. 2024. 21. P. 322–329.

London D., Morgan G.B.V.I., Acosta-Vigil A. Experimental simulations of anatexis and assimilation involving metapelite and granitic melt //Lithos. 2012. V. 153. – P. 292-307.

Lowenstern. J.B. Carbon dioxide in magmas and implications for hydrothermal systems // Miner. Deposita. 2001. V. 36. P. 490–502.

Mityaev A. S. et al. Partial Melting of Plagioclase-Free Garnet–Two-Mica Metapelite As a Model of the Formation of Ultra-Potassic Felsic Magmas under Conditions of the Continental Crust //Doklady Earth Sciences. 2022. V. 507. №. 2. P. 1064-1070.

Nicoli G., Borghini A., Ferrero S. The carbon budget of crustal reworking during continental collision: Clues from nanorocks and fluid inclusions //Chemical Geology. 2022. V. 608. P. 121025.

Safonov O. G., Khodorevskaya L. I., Spivak A.V., Kosova S.A., Viryus A.A., Yapaskurt V.O., and Voronin M. V. Graphite as an Internal Source of $CO_2$ During Crustal Anatexis: Experimental Study on Melting of Graphite-Bearing Garnet–Two Mica Schist at 500 MPa and 900°C// Petrology. 2025. Vol. 33. No. 6. P. 678–709.

Scaillet B., Macdonald R. A. Y. Phase relations of peralkaline silicic magmas and petrogenetic implications //Journal of Petrology. 2001. V. 42. №. 4. P. 825-845.

## Khodorevskaya L.I., Safonov O.G., Spivak A.V., Tushkanova S.A., Nekrasov A.N. Experimental study of partial melting graphite-containing schist at 1.0-1.5 GPa and 900°C. *UDC 552.13*

D.S. Korzhinskii Institute of Experimental Mineralogy of Russian Academy of Sciences, Chernogolovka, Moscow district khodorevskaya@mail.ru

**Abstract.** The results of experiments on the partial melting of garnet-two-mica schist with graphite at 900°C and 1.0-1.5 GPa are presented. The work aimed to investigate the effect of pressure on the potential for $CO_2$ generation from graphite-bearing metapelites under lower crustal conditions. The experimental products include the initial quartz, garnet, apatite, and ilmenite, as well as the products of peritectic melting reactions formed during the experiment: high-alumina alkali-calcium melt, potassium feldspar, rutile, and sillimanite/kyanite. Raman spectroscopy of the quenched melts obtained in the experiments revealed the presence of graphite only and the absence of carbon-containing components such as $CO_3^{2-}$ and $CO_2$. Thus, the experiments showed that at 900°C and pressures of 1.0-1.5 GPa, graphite-bearing metapelites play an insignificant role as internal sources of $CO_2$.

***Keywords**: two-mica metapelite; graphite; granitoid melts; fluids; Raman spectroscopy; $CO_2$*

**Introduction.** Safonov et al. (2025) present the results of a study of the melting of garnet-two-mica (+Qz, Ap, Ilm) schist containing varying amounts of graphite at T = 900°C and P = 0.5 GPa. In such a system, the composition of the possible fluid phase is controlled by both $H_2O$, released during the decomposition of micas, and $CO_2$, formed during the oxidation of graphite by oxygen released during the reduction of $Fe^{3+}$ and $Fe^{2+}$ in Fe-bearing minerals. Experiments demonstrate that, under high-temperature metamorphic conditions at 900°C and 0.5 GPa, graphite-bearing metapelites can effectively source $CO_2$, which accompanies granite melts during

anatexis. This paper presents the results of a study of the partial melting of the same garnet-two-mica schist with graphite at 900°C and 1.0-1.5 GPa. The work aimed to study the influence of higher pressures on the potential for $CO_2$ generation from graphite-containing metapelites in the lower crust conditions.

**Starting materials and experimental techniques.** A K5 sample of garnet-two-mica schist was used as the starting material for the experimental study. The bulk composition of the rock and the average compositions of its minerals are given in (Safonov et al., 2025, Table 1). From 2 to 10 wt.% of graphite from the Mayak mine, Norilsk ore field, was added to the shale powder. Gold ampoules were used for the experiments to avoid Fe loss into the ampoule walls. The duration time of the experiments was 5.5 days. The experiments were carried out on a cylinder-piston setup (CP-40) at the IEM RAS. NaCl cells (+ Pyrex glass for experiments above the NaCl melting curve) with a diameter of ¾ and 1/2 inch with MgO ceramic inserts and graphite heaters were used in the experiments. Oxygen fugacity was not specifically controlled during the experiments, on the assumption that this parameter was buffered by phase associations in the experimental products. According to (Patiño Douce and Harris, 1998), graphite heater cells limit the $f_{O2}$ (log units) in the sample to the range between the QFM buffer and QFM-2. A detailed description of the experimental procedure, analysis of the experimental products, study of the mineral phases compositions and obtaining Raman spectra of quenched melts are presented in (Safonov et al., 2025).

**Experimental results.** Following the experiments, changes in the composition of the original schist minerals were observed as well as the appearance of new phases, including quenched glass (Table 1). In all experiments at 1.0 GPa, muscovite disappeared. Large biotite crystals $Bt_1$ fragmented to form small prisms or worm-like clusters of $Bt_2$, which has a different composition to $Bt_1$. The amount of ilmenite decreased. It was retained in garnet and was partially or completely replaced by rutile in the melt. The garnets were zoned, retaining a lighter, more ferruginous component in the center and a more magnesian component at the margins. Along with garnet, the melt contained Al silicate (probably sillimanite) and potassium feldspar. At 1.5 GPa, the amount of newly formed Grt significantly increased in the experimental products. Kyanite and potassium feldspar were also present, as was muscovite. In places, it was flowed around by the melt, apparently partially melting, but sometimes it was preserved as large isomorphic crystals, virtually unaffected by the melt. Ilm was observed only as inclusions in Grt, and in the melt, it was completely replaced by rutile. Graphite added to the initial sample (Table 1) after all experiments forms shapeless, rounded, opaque aggregates. These aggregates may contain clusters of crystalline phases and small, rounded glass particles (however, it cannot be ruled out that these phases were introduced into the graphite during polishing).

**Table 1.** Total pressure in the experiments, graphite content in the starting mixtures and the phase composition of the run products at 900°C and pressures of 1.0-1.5 GPa.

| Run, # | Pressure, GPa | Graphite content, wt% | Run products |
|---|---|---|---|
| SK-4 | 1.0 | 2 | Gl+Kfs+Sil+Grt+Bt+Rt±Ilm+Ap +Gr+FeS |
| SK-5 | 1.0 | 5 | Gl+Kfs+Sil+Grt+Rt±Ilm+Bt+Qz+Ap+Gr+FeS |
| SK-6 | 1.0 | 10 | Gl+Kfs+Sil+Grt+Rt±Ilm+Bt+Qz+Ap+Gr+FeS |
| S4 | 1.5 | 0 | Ms+Bt+Gl+Kfs+Grt+Ky+Qz+Rt+Ap+FeS+Gr |
| S1 | 1.5 | 3 | Bt+Gl+Kfs+Grt+Ky+Qz+FeS+Gr |
| S2 | 1.5 | 5 | Ms+Bt+Gl+Kfs+Grt+Ky+Qz+Rt+FeS+Gr |
| S3 | 1.5 | 10 | Ms+Bt+Gl+Kfs+Grt+Ky+Qz+Rt+FeS+Gr |

**Note:** Gl - quenched melt, Sil – sillimanite, Ky – kyanite, Grt – garnet, Kfs - potassium feldspar, Bt- biotite, Ilm – ilmenite, Qz – quartz, Ms - muscovite, Ap – apatite, Rt – rutile, Gr - graphite.

***Garnet.*** In all experiments, the garnet grain centers were characterized by the same composition, close to the initial $Grs_{0.02}Alm_{0.91}Sps_{0.02}Prp_{0.05}$. The newly formed garnet and the rims of the initial garnet contained up to 0.7 wt% $TiO_2$ (in contrast to the initial garnet, which contained <0.01 wt% $TiO_2$), which was due to the participation of the Ti component of biotite and ilmenite in melting reactions. At 1.0 GPa in the rims of the garnet and in small newly formed garnet crystals, the pyrope minal content was X(prp) = 0.25 - 0.30; at 1.5 GPa, X(prp) = 0.17 - 0.25, with a corresponding almandine minal content, X(alm) = 0.84 - 0.69.

***Potassium feldspar*** in the experimental products contained < 1.0 wt% $Na_2O$ and <0.2 wt% CaO.

***Biotite***. Variable Ti content was observed in biotite after experiments. Large $Bt_1$ biotites, similar to the original ones, have a low Ti content. Conversely, small prisms of newly formed $Bt_2$ have a high Ti content, increasing with increasing graphite concentration from 0.3 to 0.43 f.u. at 1.0 GPa. At 1.5 GPa, the Ti content of $Bt_2$ biotite is somewhat lower, varying from 0.25 to 0.35 f.u. In addition, there are biotite varieties with intermediate titanium content.

For example, there are biotites similar in shape to $Bt_1$, but with a Ti content approaching $Bt_2$. The iron index of the mineral, F = 0.55-0.58, remains unchanged by either pressure or graphite concentration.

***Muscovite*** observed in experiments at 1.5 GPa is characterized by low Fe, Ti, and Mg contents and is virtually indistinguishable from the original (Safonov et al. 2025).

In most experiments, the appearance of FeS (the sulfur content in the original metapelite is <0.02 wt.%, Mityaev et al., 2022) in the form of very small crystals is observed (Table 1). At 1.5 GPa, their number is noticeably greater, which is obviously related to the higher degree of substitution of ilmenite by rutile.

Overall, the mineral phases of experiments conducted at both 1.0 and 1.5 GPa are generally similar, excep for the presence of stable muscovite at 1.5 GPa, variably molten Bt, and the partial or complete replacement of ilmenite by rutile.

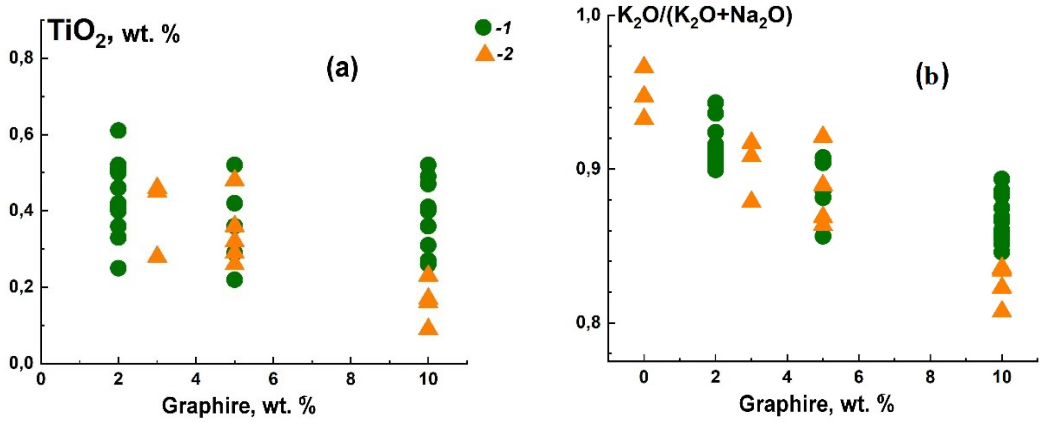


**Fig. 1a-b.** Dependence of the oxides content in the melt on the graphite content: (a) - $TiO_2$, (b) - ratio $K_2O/(K_2O+Na_2O)$: 1, 2 – 1.0 and 1.5 GPa, respectively.

***The quenched melt (glass)*** content in the experimental products is 20-30%, with a slightly lower proportion of glass at 1.5 GPa than at 1.0 GPa. The glass is heterogeneous and locally contains clusters of small sillimanite/kyanite needles. The melts are quartz-normative, with a $SiO_2$ – ($Na_2O$ + $K_2O$) ratio that is consistent with rhyolite. According to (Frost et al., 2001; Chappell et al., 2012), these are high-alumina, alkali-calcium and alkaline S-granite melts. The values of A/CNK = 1.3-1.5, A/NK = 1.4-1.6 are the same in the pressure range of 1.0-1.5 GPa and are practically independent of the graphite concentration in the initial sample. The FeO content of the melts is also independent of the graphite content and is 1.2 - 2 wt% at P = 1.0 -1.5 GPa. The $TiO_2$ content of the glass remains practically unchanged with a change in the graphite concentration in the initial sample at 1.0 GPa, but decreases at 1.5 GPa (Fig. 1a). Similarly, the $K_2O/(Na_2O+K_2O)$ ratio decreases slightly with increasing graphite content. At 1.5 GPa the decrease is more significant (Fig. 1b). This is due to the preservation of muscovite and, accordingly, the lower potassium content in the melt.

Raman spectra were obtained to determine the presence of carbon-containing components in the quenched melts. Figure 2 shows the Raman spectra of the SK-5 and C-2 experiments carried out at the same graphite content and at pressure of 1.0–1.5 GPa.

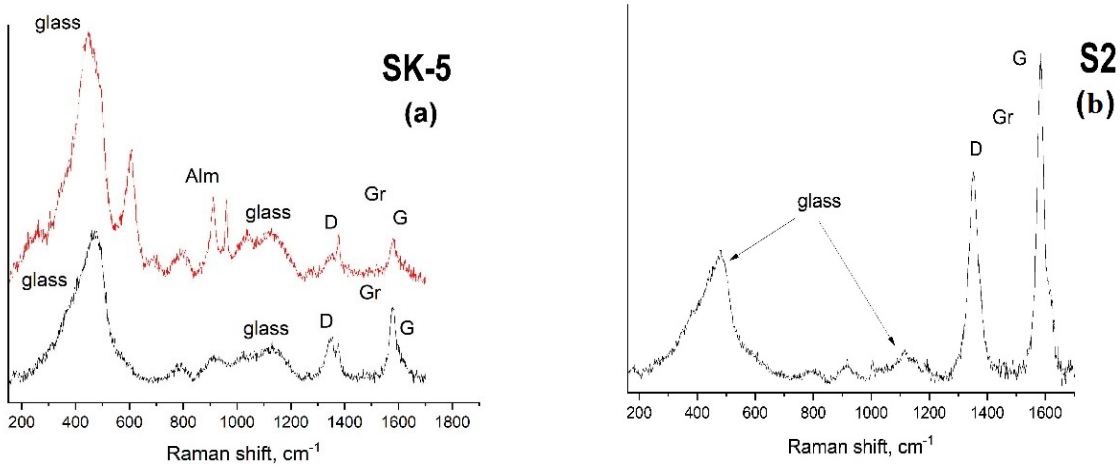


**Fig. 2.** Raman spectra of glasses in the products of experiments SK-5 (a) and S-2 (b). The D and G bands characterise the degree of disorder of the graphite (Gr) structure (Reich, Thomsen, 2004).

Broad bands of aluminosilicate glass are observed in the 900 – 1100 $cm^{-1}$ ranges, representing groups of tetrahedra with different degrees of polymerization (mainly $Q^2$ and $Q^3$; McMillan et al., 1992). Quartz band is usually present at 464 $cm^{-1}$, $OH^-$ groups in the 3450-3650 $cm^{-1}$ range (Frezzotti et al., 2012). The spectra of glasses from all samples contain D (1444 $cm^{-1}$) and G (1580 $cm^{-1}$) peaks of disordered graphite of varying intensity (Reich, Thomsen, 2004), which could be captured from the original sample. However, the glass spectrum of sample SK-5 differs slightly from the spectra of glasses from other experiments. As shown in Fig. 2a, the graphite peak D from this sample is characterized by splitting in the region of peaks at 1300–1400 $cm^{-1}$ region. The most intense characteristic Fermi dyads of $CO_2$ (~1284 and ~1388 $cm^{-1}$) are also located in this region. Therefore, $CO_2$ microinclusions may be present in the melt of this sample, despite the absence of isometric inclusions representing the gas phase in quenched melts when the sample were studied in transmitted light. Overall, the Raman spectra of the glasses obtained at different pressures and with different graphite contents were completely identical. With the exception of graphite, which was part of the initial sample, no other carbon-containing components were present.

**Discussion of experimental results.** The phase composition of the phases after the experiments indicates that complete equilibrium was not achieved in experiments lasting up to 6 days, as zoned garnets and incompletely melted micas from the original rock were still present. The complete disappearance of these micas could take a variable amount of time. For example, Pickering and Johnston (1998) shown that during the partial melting of two-mica metapelite at P = 1.0 GPa and T = 975°C for 5 days, 3-4 wt% Bt remained. At moderate pressures, melting occurs in two stages. It begins at T < 812°C according to the reaction: Ms + Bt + Pl + Qz → L + Kfs + Sil + Grt (3) until the complete depletion of Ms. Then melt formation steadily increases with increasing temperature according to the reaction: Bt + Pl + Qz + Kfs ± Sil → L + Grt (4), reaching ≈33 wt% at 975°C, 1.0 GPa. According to (Breton and Thompson 1988), these two stages apparently persist to at least 1.7 GPa, depending on the biotite composition. According to (Mityaev et al., 2022), peritectic melting products were obtained in melting experiments of the studied shale due to the following two reactions. The first reaction is expressed in the formation of more magnesian garnets Grt2 due to the decomposition of biotite: Bt + Qz + Sil = Grt + Kfs + L. The second reaction is the decomposition of ilmenite to form rutile: 3Ilm + Ky + 2Qz = Alm + 3Rt. This reaction shifts to the right with increasing pressure (Bohlen et al., 1983). Therefore, in our experiments at 1.5 GPa, complete replacement of ilmenite by rutile occurred, while at 1.0 GPa, complete replacement was not observed. The mechanism of $CO_2$ formation in graphite-bearing metapelites is associated with the presence of oxygen formed due to the reduction of $Fe^{3+} \rightarrow Fe^{2+}$ and/or $H_2O$ released during the decomposition reactions and/or partial melting of micas. At relatively low pressures (0.5 GPa), the $f_{O2}$ fugacity of the system is controlled by changes in the $Fe^{3+}/\Sigma Fe$ ratio of peritectic Fe-Mg minerals such as ilmenite, spinel, and orthoamphibole. Experiments involving the partial melting of the same metapelites at 900°C and 1.0-1.5 GPa have shown that the resulting peritectic phases (Rt, Sil/Ky, and Kfs) contain no Fe, while Grt and Ms contain only trace amounts of Fe3+. Therefore, there is no reason to expect the formation of $O_2$ through the reduction of $Fe^{3+}$ to $Fe^{2+}$ in these minerals. Biotite is the only phase in the experimental products in which the $Fe^{3+} \rightarrow Fe^{2+}$ transition is possible. However, the $Fe^{3+}/(Fe^{3+}+Fe^{2+})$ ratio in biotite is 0, indicating low $f_{O2}$ in all experiments and preventing the formation of $CO_2$.

**Conclusions**

1. Melting of garnet-two-mica metapelite at 900°C and 1.0-1.5 GPa results in the formation of high-alumina (A/CNK > 1.1) rhyolitic melts whose composition corresponds to S-type calc-alkaline granitoids. Increasing the graphite content of the initial system to 10 wt% decrease in the $K_2O/(Na_2O+K_2O)$ ratio in the melts, with this decrease being more significant at 1.5 GPa. This decrease in this ratio in the melts is associated with the stabilization of muscovite at higher pressures.

2. During partial melting of metapelite under the specified parameters, peritectic phases are represented by newly formed garnet, rutile, sillimanite, and potassium feldspar, which lack Fe. The amount of biotite in the experimental products is insignificant and it lacks $Fe^{3+}$. Therefore, the reduction of $Fe^{3+}$ to $Fe^{2+}$, the formation of $O_2$, and the formation of $CO_2$ due to graphite oxidation are excluded. Raman spectroscopy data confirm the reducing environment in the experiments, showing that only graphite and the OH group are present in the melts at 900°C and 1.0–1.5 GPa.

3. Despite the overall reducing environment arising during partial melting of metapelite at 900°C and 1.0-1.5 GPa, $f_{O2}$ in the system is partly controlled by the presence or absence of muscovite, which may be a more important factor controlling Ti solubility in the melt than pressure.

4. Experiments showed that at temperature of 900°C and pressures of 1.0-1.5 GPa, graphite-bearing metapelites play an insignificant role as internal sources of $CO_2$. Metapelites are the only effective $CO_2$ accumulators and transporters at high

temperatures of ≥900°C under conditions of Fe-containing minerals stability.

*This work was carried out within the framework of the IEM RAS research project No. FMUF-2022-0004.*

**References**

Mityaev, A.S., Safonov, A.G., Varlamov, D.A., et al., Partial melting of plagioclase-free garnet–two-mica metapelite as a model of the formation of ultrapotassic felsic magmas *under conditions of* the continental crust // Dokl. Earth Sci., 2022. V. 507. №. 2. P. 1064–1070.

Safonov O. G., Khodorevskaya L. I., Spivak A.V., Kosova S.A., Viryus A.A., Yapaskurt V.O., and Voronin M. V. Graphite as an Internal Source of $CO_2$ During Crustal Anatexis: Experimental Study on Melting of Graphite-Bearing Garnet–Two Mica Schist at 500 MPa and 900°C// Petrology. 2025. Vol. 33. No. 6. P. 678–709.

Bohlen S. R., Wall V. J., Boettcher A. L. Experimental investigations and geological applications of equilibria in the system $FeO–TiO_2–Al_2O_3–SiO_2–H_2O$ // Amer. Mineral. 1983. V. 68. № 11–12. P. 1049–1058.

Breton N. L., Thompson A. B. Fluid-absent (dehydration) melting of biotite in metapelites in the early stages of crustal anatexis // Contrib. Mineral. Petrol. 1988. V. 99. №. 2. P. 226-237.

Chappell B. W., Bryant C. J., Wyborn D. Peraluminous I-type granites // Lithos. 2012. P. 142-153.

Frezzotti M.-L., Di Vincenzo G., Ghezzo C. et al. Evidence of magmatic $CO_2$-rich fluids in peraluminous graphite-bearing leucogranites from Deep Freeze Range (northern Victoria Land, Antarctica) // Contrib. Mineral. Petrol. 1994. V. 117. P. 111–123.

Frost B.R., Frost C. D., Hulsebosch T. P. et al. Origin of the charnockites of the Louis lake Batholith, Wind River Range, Wyoming // J. Petrol. 2000. V. 41. P. 1759–1776.

McMillan P. F., Wolf G. H., Poe B. T. Vibrational spectroscopy of silicate liquids and glasses // Chem. Geol. 1992. V. 96. P. 351–366.

Patiño Douce A.E., Harris N. Experimental constraints on Himalayan anatexis // J. Petrol. 1998. V. 39. P. 689–710.

Pickering J. M., Johnston D. A. Fluid-absent melting behavior of a two-mica metapelite: experimental constraints on the origin of Black Hills granite //Journal of Petrology. 1998. V. 39. №. 10. – P. 1787-1804.

Reich S., Thomsen C. Raman spectroscopy of graphite // Phil. Trans. Royal Soc. London. Series A: Mathematical, Physical and Engineering Sciences. 2004. V. 362. P. 2271-2288.

## Korzhinskaya V.S., Suk N.I., Kotelnikov A.R., Novikov M.P., Van K.V. Solubility of hafnon in aluminosilicate melt at temperatures of 800°C, 1000°C and pressure of 400 MPa. *UDC-550.89:546.83*

D.S. Korzhinskii Institute of Experimental Mineralogy RAS, Chernogolovka vkor@iem.ac.ru; sukni@iem.ac.ru

**Abstract.** The study of the solubility of the hafnon ($HfSiO_4$) mineral in an aluminosilicate melt at temperatures of 1000°C and 800°C, a pressure of 400 MPa in the presence of water is continued. The duration of the experiments was 5 days for 1000°C and 12 days for 800°C. In the experiments, we used hafnon synthesized by us under hydrothermal conditions and granite (Orlovka deposit, well 42), which was preliminarily melted at atmospheric pressure and T = 980°C. Preliminary melted aluminosilicate glasses with different agpaitic coefficients (Kagp = (Na + K) / Al): from 0.80 to 2.5. The composition of the samples after the experiments was determined by the method of electron probe X-ray spectral analysis. A comparative analysis of the influence of agpaiticity, temperature and pressure on the solubility of hafnon in an aluminosilicate melt was carried out.

***Keywords**: aluminosilicate melt, hafnon, experiment, solubility, zirconium, hafnium*

Experimental data on the solubility of hafnon ($HfSiO_4$) in an aluminosilicate melt were obtained for temperatures of 800 and 1000°C and a pressure of 400 MPa. The experiments were carried out on a high-gas-pressure unit (UVGD-10000) in the presence of water. The duration of the experiments was 12 days for 800°C and 5 days for 1000°C. The starting material was granite (Orlovka deposit, well 42), and hafnon synthesized by the hydrothermal method at T = 600°C, P = 100 MPa from a charge of $HfO_2$ (high-purity grade) + $SiO_2$ (synthetic quartz). Pre-fused aluminosilicate glasses with different Kagp = (Na+K)/Al: from 0.80 to 2.5 were prepared. The composition of the samples after the experiments was determined using electron probe X-ray spectroscopy. The experimental methodology for elucidating the effect of agpaitic composition on the solubility of zircon and hafnon was previously described (Kotelnikov et al., 2019).

To study the dependence of zircon ($ZrSiO_4$) and hafnon ($HfSiO_4$) solubility in aluminosilicate melts of varying alkalinity on P–T parameters, we previously conducted experiments at 1000–800°C and 200 MPa in the presence of 10 wt.% $H_2O$ (Kotelnikod et al., 2020). The literature contains ample data on the solubility of zircon in aluminosilicate melts at these temperatures and pressures. Regarding hafnon ($HfSiO_4$), only studies are known (Linnen, 1998; Aseri et al., 2015), which do not allow us to draw conclusions about the effect of pressure on hafnon solubility in melt. For this purpose, we carried out experiments with hafnon for a pressure of 400 MPa at temperatures of 1000o - 800°C in the presence of water in a high-pressure

vessel with internal heating. In the experiments, we used hafnon synthesized by us under hydrothermal conditions and granite (Orlovka deposit, well 42), from the Orlovskoye deposit, Transbaikalia (well 42), with the following composition (wt.%): $SiO_2$ - 72.10; $TiO_2$ - 0.01; $Al_2O_3$ - 16.14; $Fe_2O_3$ - 0.68; MnO - 0.09; CaO - 0.30; MgO - 0.01; $Na_2O$ - 5.17; $K_2O$ - 4.28; $P_2O_5$ - 0.02; F - 0.32; $H_2O$ - 0.18, which was preliminarily melted at atmospheric pressure and T = 980 °C. Mixtures with different agpaitic indices (1.10 –2.5) were prepared from granite powder by adding appropriate amounts of $K_2CO_3$ and $Na_2CO_3$, which were melted in platinum crucibles at 1250 °C in a KO-14 furnace for 12 h and quenched into glasses of different alkalinity. The experiments were carried out in Pt ampoules with a diameter of 4 mm for T = 1000 °C and in Au ampoules (d = 3 mm) for T = 800 °C, into which a mixture of granite glass + hafnon and water was loaded. Tables 1 and 2 present the conditions and results of experiments on hafnon solubility for temperatures of 1000 °C and 800 °C at a pressure of 400 MPa.

**Table 1.** Experimental data on the solubility of hafnon in aluminosilicate melt with different agpaiticity for T = 1000°C, P = 400 MPa

| № exp. | Weight, mg | Solution, mg | $HfO_2$, wt.% | Kagp befor/exp | Kagp after/exp |
|---|---|---|---|---|---|
| Hfn-17 | 80.08 gr.+7.73Hfn | $H_2O$-69.69 | 0.31 | 1.10 | 1.02 |
| Hfn-18 | 71.48 gr.+6.72Hfn | $H_2O$-69.17 | 0.95 | 1.25 | 1.08 |
| Hfn-19 | 70.20 gr.+7.58Hfn | $H_2O$-68.49 | 3.38 | 1.50 | 1.29 |
| Hfn-20 | 70.75 gr.+7.53Hfn | $H_2O$-70.73 | 4.12 | 2.00 | 1.55 |

gr. – granite glass

**Table 2.** Experimental data on the solubility of hafnon in aluminosilicate melt with different agpaiticity for T = 800°C, P = 400 MPa

| № exp. | Weight, mg | Solution, mg | $HfO_2$, wt.% | Kagp befor/exp | Kagp after/exp |
|---|---|---|---|---|---|
| Hfn-21 | 83.67 gr.+7.41Hfn | $H_2O$ – 50.47 | 1.14 | 1.10 | 0.87 |
| Hfn-22 | 82.91 gr.+7.92Hfn | $H_2O$ – 50.38 | 1.76 | 1.50 | 1.17 |
| Hfn-23 | 81.96 gr.+6.68Hfn | $H_2O$ – 50.27 | 4.73 | 2.0 | 1.28 |
| Hfn-24 | 81.98 gr.+7.70Hfn | $H_2O$ – 48.83 | 3.69 | 2.50 | 1.44 |
| Hfn-25 | 81.21 gr.+5.01Hfn | H2O – 49.98 | 1.25 | 1.25 | 1.10 |
| Hfn-26 | 81.41 gr.+8.51Hfn | H2O – 49.60 | 6.29 | 2.30 | 1.62 |

gr. – granite glass

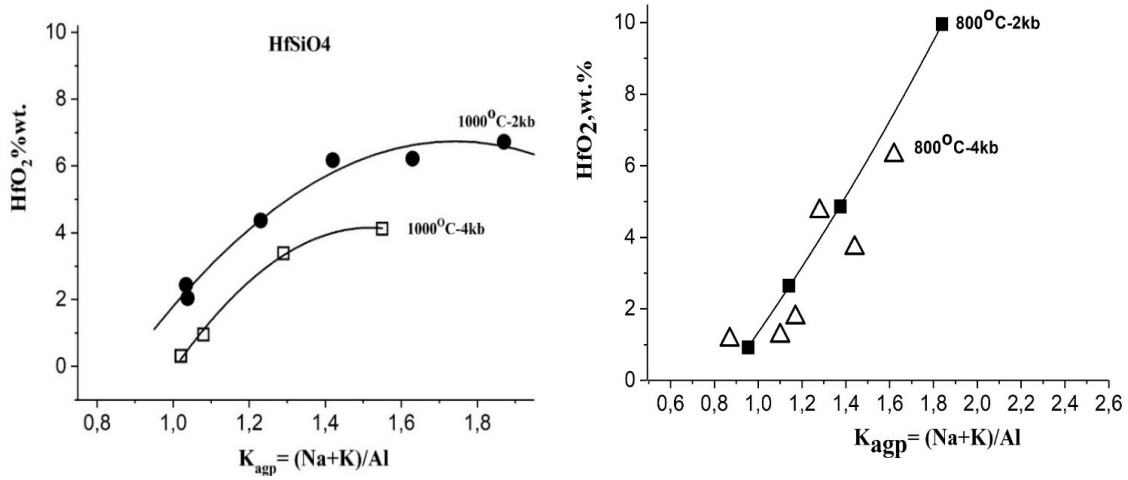


**Fig. 1.** Dependence of hafnon solubility on agpaiticity (Kagp = (Na+K)/Al) in an aluminosilicate melt in the presence of water (T = 1000°C, 200 – 400 MPa).

**Fig. 2.** Dependence of hafnon solubility on agpaiticity (Kagp = (Na+K)/Al) in an aluminosilicate melt in the presence of water (T = 800°C, 200 – 400 MPa)

.

We previously studied the solubility of hafnon at temperatures of 1000°C and 800°C and a pressure of P = 200 MPa in the presence of water (Kotelnikov et al., 2020). **Figure 1** shows the dependence of hafnon solubility on agpaiticity for pressures of 200 and 400 MPa. It was found that hafnon solubility depends on the composition of the aluminosilicate melt, increasing with increasing agpaiticity ((Na + K)/Al). At the same time, the agpaiticity coefficient in a water-containing system decreases compared to the

initial value, which can be explained by the partial redistribution of alkalis into the fluid phase. Thus, for Kagp befor/exp = 1.50, the agpaiticity coefficient after the experiment decreases to 1.29, and the $HfO_2$ content in the glass is 3.38 wt%. For this temperature at a pressure of 200 MPa, the HfO2 content in the glass is 6.59 wt.%, and the initial Kagp befor/exp = 1.50 decreased to Kagp after/exp = 1.40.

For a temperature of 800°C and a pressure of 400 MPa, **Table 2** presents the experimental conditions and results, and **Fig. 2** compares the $HfO_2$ content in silicate glass at 200 and 400 MPa. For T = 800°C, the effect of pressure is more noticeable. For example, for an initial agpaitic index of Kagp = 1.50, the agpaitic index decreased to Kagp = 1.17, while the $HfO_2$ content was 1.76 wt.%. At 200 MPa, for this temperature, the initial agpaitic index decreased to Kagp = 1.38, and the HfO2 content in the glass was 2.5 times higher, amounting to 4.86 wt.%. **Tables 3 and 4** present the probe compositions of the experimental glasses obtained at 1000°C and 800°C, and a pressure of 400 MPa.

**Figure 3** shows a comparison plot of hafnon solubility in an aluminosilicate melt at temperatures of 800°C and 1000°C and a pressure of 400 MPa. The plot shows that hafnon solubility in glass decreases with increasing temperature, while the agpaitic coefficient in the aqueous system decreases more rapidly at 1000°C, which can be explained by the greater redistribution of alkalis into the fluid phase. For 800°C, the scatter of points likely also results from the uneven redistribution of alkalis into the fluid.

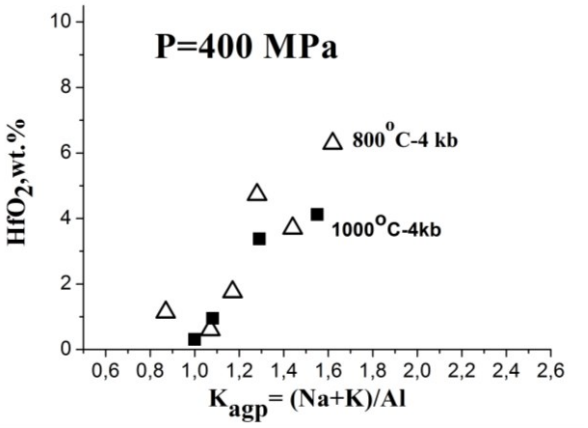


**Fig. 3** Dependence of hafnon solubility on agpaiticity (Kagp = (Na+K)/Al) in an aluminosilicate melt in the presence of water for temperatures of 800°C and 1000°C and a pressure of 400 MPa.

**Table 3.** Electron probe composition (in wt.%) of glass after experiments for hafnon ($HfSiO_4$) at 1000°C and a pressure of 400 MPa

| Elements | Hfn-17 | Hfn-18 | Hfn-19 | Hfn-20 |
|---|---|---|---|---|
| | 1000°C, 400 MPa | | | |
| $Na_2O$ | 4.71 | 3.90 | 4.50 | 5.87 |
| $Al_2O_3$ | 12.95 | 11.54 | 11.20 | 10.99 |
| $SiO_2$ | 61.64 | 67.47 | 63.38 | 55.14 |
| $K_2O$ | 4.84 | 5.57 | 6.45 | 6.60 |
| CaO | 0.10 | 0.14 | 0.156 | 0.09 |
| $TiO_2$ | 0.09 | 0.06 | 0.07 | 0.04 |
| MgO | 0.04 | 0.08 | 0.05 | 0.06 |
| MnO | 0.10 | 0.06 | 0.06 | 0.07 |
| FeO | 0.09 | 0 | 0.102 | 0.03 |
| $ZrO_2$ | 0.16 | 0.10 | 0.10 | 0.14 |
| $HfO_2$ | 0.31 | 0.95 | 3.38 | 4.12 |
| F | 0.21 | 0.2 | 0.17 | 0.12 |
| Total | 85.03 | 89.81 | 89.62 | 83.29 |
| Kagp befor/exp | 1.10 | 1.25 | 1.50 | 2.0 |
| Kagp after/exp | 1.02 | 1.08 | 1.29 | 1.55 |

**Table 4.** Electron probe composition (in wt.%) of glass after experiments for hafnon ($HfSiO_4$) at 800°C and a pressure of 400 MPa

| Elements | Hfn-21 | Hfn-22 | Hfn-23 | Hfn-24 | Hfn-25 | Hfn-26 |
|---|---|---|---|---|---|---|
| | 800°C, 400 MPa | | | | | |
| $Na_2O$ | 4.87 | 3.99 | 4.27 | 5.72 | 3.58 | 5.92 |
| $Al_2O_3$ | 15.65 | 11.17 | 12.20 | 12.99 | 11.15 | 10.70 |
| $SiO_2$ | 64.82 | 62.39 | 57.60 | 52.75 | 65.60 | 56.53 |
| $K_2O$ | 5.14 | 5.83 | 7.84 | 8.59 | 5.53 | 7.22 |
| CaO | 0.08 | 0.06 | 0.21 | 0.09 | 0.17 | 0.10 |
| $TiO_2$ | 0.02 | 0.07 | 0.04 | 0.03 | 0.12 | 0.16 |
| MgO | 0.15 | 0.06 | 0.08 | 0.12 | 0.07 | 0 |
| MnO | 0.13 | 0.03 | 0.03 | 0.02 | 0.06 | 0.15 |
| FeO | 0.45 | 0.03 | 0.06 | 0.08 | 0.11 | 0.21 |
| $ZrO_2$ | 0.02 | 0.02 | 0.11 | 0.04 | 0.12 | 0 |

| Elements | Hfn-21 | Hfn-22 | Hfn-23 | Hfn-24 | Hfn-25 | Hfn-26 |
|---|---|---|---|---|---|---|
| | 800°C, 400 MPa | | | | | |
| $HfO_2$ | 1.14 | 1.76 | 4.73 | 3.69 | 1.25 | 6.29 |
| F | 0.39 | 0 | 0.15 | 0.16 | - | 0.15 |
| Total | 92.66 | 85.41 | 87.32 | 84.24 | 87.39 | 87.30 |
| Kagp befor/exp | 1.10 | 1.50 | 2.00 | 2.50 | 1.25 | 2.3 |
| Kagp after/exp | 0.87 | 1.17 | 1.28 | 1.44 | 1.10 | 1.62 |

According to literature data (Linnen, 1998; Van Lichtervelde et al. 2010; Aseri, A.A et al., 2015) and our experiments (Kotelnikov et al. 2020), it was found that melt composition and temperature have a greater effect on the solubility of hafnon ($HfSiO_4$) compared to pressure.

*This study is fulfilled under Research program FMUF–2022-0004 of the D.S.Korzhinskii Institute of Experimental Mineralogy*

**References:**


**1**. Kotelnikov A.R., Korzhinskaya V.S., Suk N.I., Van K.V., Virus A.A**.** Experimental study of zircon and loparite solubility in silicate melt // Experiment in Geosciences, 2019, Volume 25, N 1, P.P.138 - 140. (ISSN: 0869-2904).

**2.** Kotelnikov A.R., Korzhinskaya W.S., Suk N.I., Van K.V. Experimental study of zircon and hafnon solubility in silicate melts // ExperGeos, 2020, vol. 26, №1, p.p. 155-158.

**3.** Aseri, A.A., Linnen, R.L., Che, X.D., Thibault, Y., and Holtz, F., Effects of fluorine on the solubilities of Nb, Ta, Zr and Hf minerals in highly fluxed water-saturated haplogranitic melts, *Ore Geol. Rev.,* 2015, vol. 64, pp. 736-746.

**4**. R.L. Linnen The solubility of Nb-Ta-Zr-Hf-W in granitic melt with Li and Li-F // Economic Geology. 1998, vol. 93, p.p.1013-1025.

**5**. Marieke Van Lichtervelde. Francois Holtz., John M. Hanchar. Solubility of manganotantalite, zircon and hafnon in highly fluxed peralkaline to peraluminous pegmatitic melts// Contrib Mineral Petrol. 2010. 60:17–32**.** DOI 10.1007/s00410-009-0462-x


## Kotelnikov A.R.[1], Suk N.I.[1], Kotelnikova Z.A.[2], Krinochkina O.K.[3], Drozhzhina N.A.[1], Van K.V.[1] Study of albitization processes: experimental data. *UDC 550.89:550.46*

[1] IEM RAS, Chernogolovka, Moscow region; [2] IGPMG RAS, Moscow; [3] MSCU, Moscow
kotelnik1950@yandex.ru; sukni@iem.ac.ru

**Abstract.** An experimental study of albitization was conducted in hydrothermal solutions at a temperature of 650-680°C and a pressure of 4 kbar. Basaltic and plagioclase glasses ($An_{80}$ and $An_{60}$) as well as synthetic quartz powder were used as starting materials. Solutions of salts $(K,Na)Cl+(K,Na)_2CO_3+NH_4Cl$ with a concentration of ~30 wt% were used, with the addition of a certain amount of 5% alkali solution (KOH, NaOH). It was shown that albitization of both basalts and plagioclases occurs according to the following reactions:

$$CaAl_2Si_2O_8 + Na_2CO_3(aq)+4SiO_2(aq) = 2NaAlSi_3O_8+CaCO_3\downarrow \quad (1)$$

$$CaAl_2Si_2O_8 + NaSiO_3(aq) + 4SiO_2(aq) = 2NaAlSi_3O_8 +CaSiO_3\downarrow \quad (2)$$

The experimental products contained minerals such as clinopyroxenes, carbonates, and quartz. In the presence of sulfides, typical ore assemblages formed in albitites: Ab + Qz + Cpx + Cb + MeS. It was shown that albitization processes occur under the influence of alkaline fluids during postmagmatic metamorphic processes.

***Keywords**: albitization, hydrothermal solution, ore assemblages, experiment*

**Introduction**. Albitization refers to a metasomatic process in which, under the influence of high-temperature hydrothermal solutions, the original rock minerals are replaced by albite and, sometimes, potassium feldspar. As a result, the original rock becomes enriched in sodium (potassium), and to some extent depleted in divalent bases (Ca, Mg, Mn, $Fe^{2+}$). Albitization processes are typically associated with residual fluids during the crystallization of granite massifs, and therefore are most often confined to the apical parts of batholiths. Thus, the parameters of this process are as follows: temperature 650 → 150 °C, pressure 4 → 1 kbar. Fluids during albitization are alkaline in nature with the participation of carbon dioxide and can be represented by the system $(Na,K)Cl + (Na,K)_2CO_3 + H_2O + CO_2$. Enrichment of the fluid system with alkali metal carbonates (P-Q type salts) led to increased solubility of silicate minerals and relatively high $SiO_2$(aq) concentrations in the albitizing fluid. The presence of such P-Q type solutions (Ravich, 1977) suggests heterogeneity and phase inhomogeneity of these fluids. A typical paragenesis of albitized rocks is albite + quartz ± amphibole ± chlorite (epidote) + carbonate ± ore mineral. Albitization zones often develop in the apical parts of intrusive rock massifs. Such intrusive complexes can be associated with zones of collision of continental lithospheric plates, the final stages of the development of orogenic belts, magmatic arcs of active margins of continental plates, zones of deep

faults and rift systems. However, areal albitization processes also occur, occurring during diaphthoresis of metamorphic and volcano-sedimentary rocks. The accumulation, transport, and deposition of ore minerals during albitization can be one criterion for the potential ore content of "parent" rocks (intrusives). Therefore, it was highly desirable to conduct experimental modeling of the albitization process to study the albitization reactions themselves and their chemical properties.

**Experimental method**. Experimental studies of albitization were conducted in hydrothermal solutions at temperatures of 650–680°C and pressures of 2–4 kbar. Several experiments were carried out under thermal gradient conditions: the temperature at the bottom of the ampoule was 30–40°C higher than at the top. Basaltic glass from the East Pacific Rise served as starting materials; the basaltic glass composition (wt%) was: $SiO_2$ – 47.65; $TiO_2$ – 2.05; $Al_2O_3$ – 13.04; FeO – 11.26; MnO – 0.10; CaO – 10.51; MgO – 6.02; $Na_2O$ – 2.79; $K_2O$ – 0.05; $SO_3$ – 0.52; sum 93.98. In addition, specially prepared plagioclase glasses ($An_{80}$ and $An_{60}$) were used. Their compositions are as follows (wt.%) – $An_{60}$: $SiO_2$ – 53.05, $Al_2O_3$ – 30.03, CaO – 12.39; $Na_2O$ – 2.56, $K_2O$ – 0.03, sum 100.04; $An_{80}$: $SiO_2$ – 48.05, $Al_2O_3$ – 33.34, CaO – 16.31; $Na_2O$ – 2.25, $K_2O$ – 0.02, sum 99.98. Synthetic quartz powder was added to the starting mixture. Solutions of a salt mixture of (K,Na)Cl+$(K,Na)_2CO_3$+$NH_4Cl$ were used, with concentrations of up to ~30-35 wt.%, sometimes with the addition of a small amount of a 5% (K,Na)OH solution. Thus, the initial solution was alkaline.

All experiments were carried out on high-gas-pressure units (HGPU) designed by the IEM RAS. Hydrothermal units with external heating and a cold seal were also used. The accuracy of temperature control and regulation was ±2°C, pressure ±50 bar. The start-up time was ~1 hour, and the quenching of the experiment took 3-5 minutes. The duration of the experiments was 14-15 days. The tightness of the ampoules was checked by the gravimetric method. The experiments were carried out in gold (5x0.2x50mm or 8x0.2x70mm) and platinum (7x0.2x70mm) ampoules. Salts and the initial sample were loaded into the experiments, and the required amount of solution was poured in. The ampoule was welded, weighed, placed in the HGPU reactor, and maintained in the experimental mode for 14-15 days.

The compositions of the mineral products of the experiments were studied by the method of micro-X-ray spectral analysis on a Tescan Vega II XMU electron microscope (Czech Republic), equipped with energy-dispersive (INCAx-sight) and crystal diffraction (INCA wave) X-ray spectrometers (England, Oxford). X-ray diffraction study of the experimental products was performed on HZG-4 and "Bruker" diffractometers in continuous scanning mode. Spectral-purity silicon (a=5.4307 [Å]) was used as an internal standard. The polygonal method of X-ray reflection correction was used (Kroll e.a., 1995; Kotelnikov, 1995). The obtained results allowed us to calculate the unit cell parameters of the solid solutions. The unit cell parameters were refined using 45–103 reflections in the angular range of 6.5–44.5° (Θ). The parameters were calculated using the LCC, PUDI, and MINCRYST programs (Burnham, 1991; Chichagov, 1994).

**Study of albitization (calispatization) processes of basalts.**

The experimental conditions are shown in Table 1. The experiments lasted 14-15 days. Platinum ampoules measuring ø7x0.2x60 were used.

**Experiment 7368.** The experimental products contained albite, clinopyroxene, quartz, and sphalerite. Carbonate crystals – calcite with a small admixture of iron were occasionally encountered. Sphalerite contains up to 2.3 wt.% Fe (about 4 mol.%). Albite contains small amounts of potassium (up to 1 mol.%) and iron. Its crystal chemical formula (based on 8 [O] atoms) is: $(Na_{0,95}K_{0,01})_{0.96}(Al_{0.99}Si_{3.02})_{4.01}O_8$.

The average composition of clinopyroxenes from the experimental products (recalculated to 6 atoms [O]) corresponds to the following formula: $(Na_{0.30}Ca_{0.76}Mg_{0.48}Fe_{0.51}Al_{0.08})_{2.13}(Al_{0.05}Si_{1.95})_{2.00}O_6$. This Cpx contains 22 mol.% of aegirine endmember, its magnesium content $X_{Mg}^{Cpx}=Mg/(Mg+Fe^{2+}) = 0.62$. We calculated the composition of clinopyroxene, corresponding to the composition of basalt during crystallization of the melt of this basalt at 5 kbar with a water content in the melt of 0.2 wt.% using the Petrolog-3 program (Danyushevsky, Plechov, 2011). The formula for this Cpx (in terms of 6 [O] atoms) is as follows: $(Na_{0.04}Ca_{0.81}Fe_{0.49}Mg_{0.69}Al_{0.10})_{2.13}(Al_{0.01}Si_{1.99})_{2.00}O_8$, $X_{Mg}^{Cpx}=0.58$. The calculated composition of plagioclase obtained by modeling basalt crystallization (crystal chemical formula for 8 [O] atoms) is $(Na_{0.68}Ca_{0.32})_{1.00}(Al_{1.32}Si_{2.68})_{4.00}O_8$. It can be concluded that during albitization (under conditions of excess silica), plagioclase of the $An_{32}$ composition became pure albite, and clinopyroxene increased its magnesium number (from 0.58 to 0.62) and increased its sodium content due to the formation of an aegirine end member. Calcium, removed from Pl and Cpx under carbonate fluid conditions, formed calcite crystals.

**Table 1.** Parameters of experiments to study albitization processes under hydrothermal conditions

| N sample | $T_{low}$, °C | $T_{up}$, °C | Initial load | Initial solution | Experimental products |
|---|---|---|---|---|---|
| 7368[1)] | 680 | 650 | 200mg bas.VTP[2)] +sm3894 +100 mg ZnS + Fsp[3)] + Qz | 100 mg NaCl+100 mg $Na_2CO_3$ +50 mg $NH_4Cl$ +460 mg $H_2O$ | Ab+Qz+Cpx+ Cc + Sph[4)] |
| 7369 | 680 | 650 | -"- | 200 mg KCl+200 mg $K_2CO_3$ + 100 mg $NH_4Cl$ +720 mg $H_2O$ | Ksp+Qz +Sph +Gln+Cc (less) |
| 7651 | 650 | 650 | 200 mg glass $An_{80}$ + 100 mg Qz | 40 mg NaCl + 40 mg $Na_2CO_3$ +10 mg $NH_4Cl$ +180 mg $H_2O$+ 10 mkl 1M NaOH | Ab+Lab+Wol + Cc + Qz |
| 7653 | 650 | 650 | 200 mg glass $An_{60}$ + 100 mg Qz | 40 mg NaCl + 40 mg $Na_2CO_3$ +10 mg $NH_4Cl$ +180 mg $H_2O$+ 10 mkl 1M NaOH | Ab+Olig+Wol+Qz |

[1)] The pressure in experiment 7368, 7369 was 4 kbar; in experiment 7651, 7653 – 2 kbar; [2)] bas.VTP – basalt of the East Pacific Rise, sm3894 – smoker sulfides (Sph + Cpy); [3)] Fsp – glass $(Na_{0.75}K_{0.25})AlSi_3O_8$ ; [4)] Mineral indices: Ab – albite, An – anorthite, Cc – calcite, Cpx – clinopyroxene, Cpy – chalcopyrite, Fsp – feldspar, Gln – galenite, Ksp – potassium feldspar, Lab – labradorite, Olig – oligoclase, Qz – quartz, Sph – sphalerite, Wol – wollastonite.

**Experiment 7369.** The experimental products revealed only potassium feldspar, quartz, calcite, sphalerite, and galenite. This is likely due to the higher chemical activity of potassium. Sphalerite occurs in intergrowths with feldspar (Fig. 1). Sphalerite contains up to 5.7 wt.% Fe, with the following formula: $(Zn_{0.90}Fe_{0.10})S$. Galenite contains small amounts of zinc – up to 0.7% by weight. The formula of galenite is: $(Pb_{0.97}Zn_{0.03})S$. Potassium feldspar is almost pure, formula: $(K_{1.02}Na_{0.02})_{1.04}(Al_{0.97}Si_{3.01})_{3.98}O_8$.

Thus, in this experiment, elements such as Ca, Fe, Mg, Mn passed into solution, partially entering into calcium carbonate.

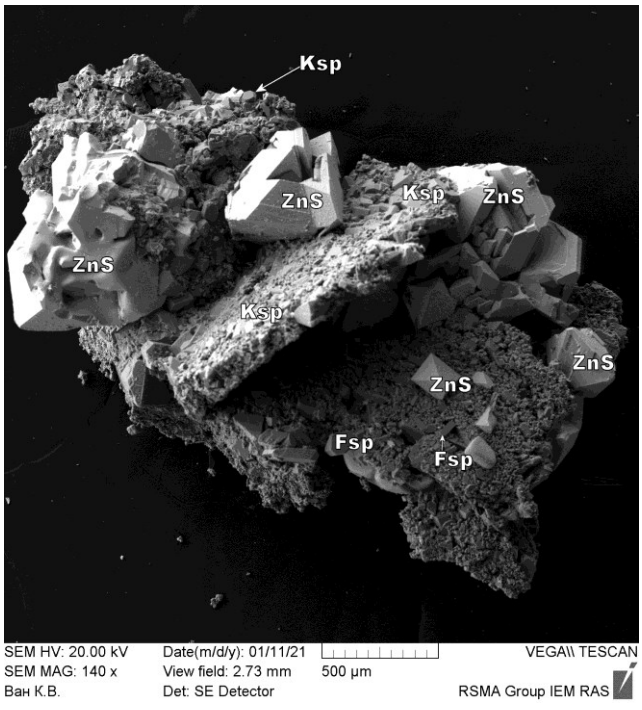


**Fig. 1.** Intergrowths of potassium feldspar (Ksp, Fsp) and sphalerite (ZnS). Sample 7369.

**Study of albitization processes of plagioclase glasses.** The experimental conditions are presented in Table 1. For experiment 7651 (initial composition $An_{80}$), feldspar – plagioclase, wollastonite, calcite, and quartz were detected in the experimental products. Most of the plagioclase grains were represented by albite, its formula (calculated per 8 [O]) is as follows:

$(Na_{0.95}K_{0.02}Ca_{0.15})_{1.12}(Al_{1.02}Si_{2.86})_{3.88}O_8$;

$X_{Ca}^{Pl}$=0.13±0.05. This sample contains plagioclase grains, similar in composition to labradorite, their formula (8 atoms [O]): $(Na_{0.56}Ca_{0.51}K_{0.02})_{1.09}(Al_{1.55}Si_{2.44})_{3.99}O_8$;

$X_{Ca}^{Pl}$=0.47±0.15. Wollastonite containing up to 0.8 wt.% FeO and 0.3 wt.% $Al_2O_3$ with the formula $Ca_{0.99}Fe_{0.01}Al_{0.01}Si_{0.99}O_3$ is also present in the experimental products, along with calcite and quartz. A similar mineral assemblage is also present in experiment 7653 (with the initial $An_{60}$).

Based on the experiments, it can be concluded that albitization of both basalts and plagioclases occurs via the following reactions:

$CaAl_2Si_2O_8 + Na_2CO_3(aq) + 4SiO_2(aq) = 2NaAlSi_3O_8 + CaCO_3\downarrow$ (1)

$CaAl_2Si_2O_8 + NaSiO_3(aq) + 4SiO_2(aq) = 2NaAlSi_3O_8 + CaSiO_3\downarrow$ (2)

In addition to albite and quartz, minerals such as wollastonite and calcite are synthesized during albitization.

The unit cell parameters of the phases synthesized during albitization of minerals were calculated and are listed in Table 2. The plagioclases formed during the experiments are structurally disordered. Their compositions were shown to vary from $An_5$ to ~$An_{50}$, indicating that the experiments were not long enough for reactions (1) and (2) to proceed to completion.

**Table 2.** Parameters of the elementary cells of the phases from the experimental products

| № | Phase | $X_{Ca}^{Fsp}$ | n | a, [Å] | b, [Å] | c, [Å] | α, [°] | β, [°] | γ, [°] | V, [Å $^3$] |
|---|---|---|---|---|---|---|---|---|---|---|
| 7651 | Ab | 0.129 | 44 | 8.153 | 12.842 | 7.119 | 93.67 | 116.45 | 89.60 | 665.8 |
| 7651 | Lab | 0.466 | 40 | 8.166 | 12.863 | 7.105 | 93.44 | 116.08 | 90.49 | 668.5 |
| 7651 | Wol | - | 35 | 7.926 | 7.328 | 7.052 | 90.31 | 95.24 | 103.47 | 396.6 |
| 7653 | Ab | 0.077 | 47 | 8.152 | 12.848 | 7.116 | 93.76 | 116.42 | 89.63 | 665.8 |
| 7653 | Olig | 0.432 | 50 | 8.166 | 12.850 | 7.113 | 93.44 | 116.10 | 90.14 | 668.7 |
| 7653 | Wol | - | 37 | 7.933 | 7.330 | 7.050 | 90.19 | 95.25 | 103.51 | 396.8 |

**Conclusions**

1. Experimental modeling of albitization processes was conducted using mafic plagioclase glass and basalt glass as starting materials.

2. It was shown that albitization occurs in alkaline solutions in the presence of dissolved $SiO_2$.

3. During albitization, minerals such as albite + quartz + pyroxene + calcite are formed.

4. Alkaline solutions, which cause albitization, also transport ore components. Therefore, albitization of rocks can serve as a prospecting indicator of ore-generating processes.

This work was supported by the IEM RAS Research Program No. FMUF-2022-0003.

**References:**

1. Kotelnikov A.R. Isomorphism in framework aluminosilicates. Abstract of a dissertation by Doctor of Geological and Mineral Sciences. Moscow. 1995. 36 p.
2. Ravich M.I. Water-salt systems at elevated temperatures and pressures. Moscow: Nauka. 1974. 151 p.
3. Burnham C.W. Least-squares refinement of crystallographic lattice parameters for IBM PC/XT/AT and compatibles. Harward University, Cambridge MA02138, 1991 (program description, 24p.)
4. Chichagov A.V. Information-calculating system on crystal structure data of minerals (MYNCRYST)// Materials Science Forum, volks 166-169, 1994. Trans. Tech. Publications. Switzerland. 1994. P.187-192.
5. Danyushevsky L.V., Plechov P. Petrolog 3: Integrated software for modeling crystallization processes // Geochem. Geophys. Geosyst., 2011, v. 12, Q07021, doi:10.1029/2011GC003516.
6. Kroll H., Kotelnikov A.R., Goettlisher J., Valyashko T.V. (K,Sr)- feldspar solid solutions: the volume behavior of heterovalent feldspars. Eur. J. Mineral., 1995. V.7. P. 489-499.

**Persikov E.S.[1*], Bukhtiyarov P.G.[1**], Aranovich L.Y.[1,2***], Sultanov D.M.[1****], Shaposhnikova O.Y.[1*****], Nekrasov A.N.[1******] Features of crystallization of basalt melt at moderate methane-hydrogen fluid pressures (preliminary results).** *UDC 123.456*

[1] D.S. Korzhinsky Institute of Experimental Mineralogy, Russian Academy of Sciences, Chernogolovka, Moscow Region, Russia ; [2] Institute of Geology of Ore Deposits, Petrography, Mineralogy and Geochemistry of the Russian Academy of Sciences, Moscow, Russia, *persikov@iem.ac.ru, **pavel@iem.ac.ru, ***lyaranov@igem.ru, ****Dilshod.Soultanov@iem.ac.ru, *****zakrev@iem.ac.ru, ******alex@iem.ac.ru

**Abstract.** Important problems of magma differentiation, the formation of native metals, and the processes of ore formation in the earth's crust are increasingly associated with the active participation of reducing fluid ($CH_4$ + $H_2$). In this work, new experimental data on the crystallization of basalt melts at high temperatures (1100–1250 °C) have been obtained) and reducing fluid pressures (10–100 MPa), which clarify the possible role of reducing fluid in the processes occurring in basalt melts in the earth's crust and during volcanism under highly reducing conditions f($O_2$) = $10^{-14}$ MPa. In crystallization experiments, it was found that the compositions of crystals (olivines, clinopyroxenes and plagioclase) formed in the experiment on crystallization of magnesia basalt melt under fluid pressure ($CH_4$ + $H_2$) closely correspond to the composition of crystals of lava flows of the northern eruption of the Tolbachik volcano in Kamchatka. This result can be considered as experimental confirmation of the participation of reducing fluid in the volcanic process.

***Keywords**: basalt, melt, hydrogen + methane, pressure, temperature, native metal, liquation, crystallization, reducing conditions*

In Russia, large-scale manifestations of native iron have been found in the Arctic, in the north of the Krasnoyarsk Territory, in the trap intrusives of the Jaltulsky, Khungtukunsky, Khinindinsky, and Maymechinsky (Oleynikov et al., 1985; Ryabov et al., 1985; Tomshin et al., 2023; et al.). Native iron forms gland-like segregations, in which cogenite, troilite, and magnetite-wüstite are present in subordinate amounts. Ni, Co, Au and PGE are actively concentrated in metallic iron. It has been established that their content in the metal increases by hundreds and even thousands of times compared to the host silicate rock (Tomshin et al., 2023). According to Yakut geologists, the formation of native iron is based on the fluid-magmatic interaction of magma matter with the reducing components of the fluid, mainly of methane-hydrogen composition (Oleynikov et al., 1985; Tomshin et al., 2023; et al.). This paper presents new experimental data on the crystallization of basalt melts at high temperatures (1100–1250 °C) and reducing fluid pressure (10–100

MPa), which clarify the possible role of hydrogen in the processes occurring in basalt melts in the earth's crust and during volcanism under highly reducing conditions $f(O_2) = 10^{-14}$ MPa.

The experiments were carried out using a unique high-gas pressure unit equipped with an original internal device, which made it possible to conduct long-term experiments at high temperatures, despite the high penetrating power of hydrogen (Fig. 1).

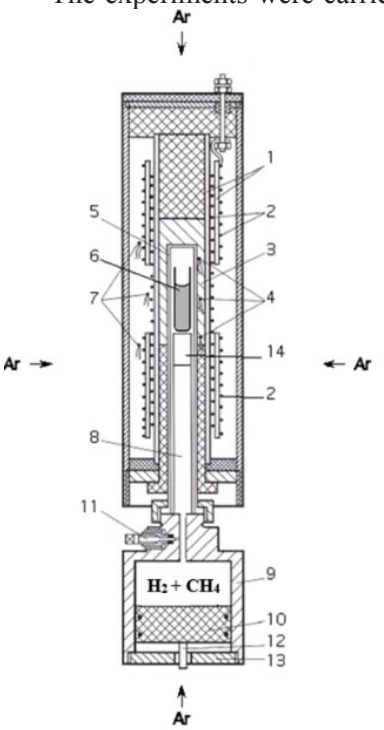


**Fig. 1**. Diagram of a unique internal device with an internal heater of a high-pressure vessel.

1, 3 - insulators; 2 - two heater windings; 4 - three thermocouples to control the temperature gradient along the ampoule with the sample; 5 - molybdenum reactor ; 6 - alund ampoule with the sample (melt); 7 - two thermocouples to control the temperature of each heater winding; 8 - sapphire cylinder; 9 – equalizer-separator body; 10 – equalizer-separator piston; 11 – shut-off valve; 12 – piston position control sensor; 13 – cover; 14 – alund ampoule with tantalum wire

**Table 1.** Chemical composition (wt. %) and structural-chemical parameter (100NBO/T) of the initial basalt and basalt glass (average composition) after methane-hydrogen fluid pressure experiments.

| Components | 2128* | 2126** | Composition of the original basalt*** |
|---|---|---|---|
| $SiO_2$ | 54.05 | 55.86 | 49.5 |
| $Al_2O_3$ | 14.79 | 16.75 | 13.18 |
| $Fe_2O_3$ | 0.00 | 0.00 | 3.18 |
| FeO | 4.32 | 6.79 | 6.85 |
| MnO | 0.16 | 0.15 | 0.15 |
| MgO | 9.26 | 3.41 | 9.98 |
| CaO | 12.36 | 9.68 | 12.34 |
| $Na_2O$ | 2.65 | 3.34 | 2.18 |
| $K_2O$ | 1.0 | 1.96 | 0.93 |
| $TiO_2$ | 1.17 | 1.26 | 1.01 |
| $P_2O_5$ | no | 0.2 | 0.25 |
| $H_2O$- | 0.3 | 0.3 | 0.29 |
| NiO | 0.07 | 0.07 | no |
| $Co_3O_4$ | 0.1 | 0.1 | no |
| **Sum** | 100.23 | 99.87 | 99.84 |
| 100NBO/T | 74 | 44 | 83 |

**Note:** The water content is determined by Karl-Fischer titration

* - Experiment with molten magnesian basalt: P(fl.) = 100 MPa, T = 1250 °C, exposure for 1 hour, then reduction of fluid pressure to 10 MPa in isothermal mode, exposure for 1 hour, and then isobaric quenching.

** - Experiment with molten magnesian basalt: P(fl.) = 100 MPa, T = 1250 °C, exposure for 1 hour, then reduction of fluid pressure to 10 MPa in isothermal mode, exposure for 1 hour, then temperature reduction to 1100 °C, exposure for 2 hours (crystallization) and then isobaric quenching.

*** - Magnesian basalt of the northern breakthrough of Tolbachik volcano, eruption of 1975-1976, Kamchatka (Fedotov et al., 1984).

The device includes a molybdenum reactor with a molybdenum ampoule with an initial sample placed in it. The internal volumes of the molybdenum reactor and the equalizer-separator under the piston were filled with a methane – hydrogen mixture at a pressure of 10 MPa using a special system. Due to the movement of the piston of the equalizer-separator, the fluid pressure in the internal volume of the molybdenum reactor was always kept equal to the gas pressure (Ar) in the vessel during the experiment.

The error in measuring the temperature of the experiment was ± 5°C, and the fluid pressure ± 0.1 % of the relation. In the experiments, natural samples of igneous rocks were used: magnesian basalt of the northern breakthrough of Tolbachik volcano (Kamchatka), as well as magnesian basalt enriched with oxides of nickel and cobalt (Table 1).

The chemical composition of the samples after the crystallization experiments in comparison with

the initial composition of magnesian basalt is shown in Table 1. To compare the initial composition of the melts with the compositions of the experimental products, not only the difference in the concentrations of the main rock-forming components was used, but also the gross basicity of the melts, which is numerically determined using the structural-chemical parameter 100NBO/T - the degree of depolymerization or the coefficient of basicity, where T is the sum of the gram-ions forming the melt network ($Si^{4+}$, $A1^{3+}$, $Fe^{3+}$, $Ti^{4+}$, $P^{4+}$, $B^{3+}$), which are in tetrahedral coordination with oxygen and are part of the anionic part of the melt structure; NBO is the total number of gram ions of non-bridging oxygen in the melt. This structural-chemical parameter of melts quite correctly reflects the basicity of magmatic melts and, accordingly, the features of the gross chemical composition and structure of magmatic melts, which was substantiated in detail earlier (e.g., Persikov et al., 2020). The composition of the metallic phase formed in the experiments is shown in Table 2.

On the basis of experimental modeling, the following features of the process of interaction of reducing fluid with basalt melts have been established. In both types of experiments, it was found that, despite the high reduction potential of the methane hydrogen fluid – basalt melt system – $lgf(O_2)$ = -14, the reactions of hydrogen oxidation and complete reduction of Fe oxides in the melt do not end. As a result, the initially homogeneous basalt melt becomes heterogeneous (Table 1): $H_2O$ is formed in the fluid phase (initially anhydrous fluid); $H_2O$ dissolves in basalt melts, and small isolations of the metal of the liquation structure are formed at a temperature much lower (1250 °C) than the melting point of the metal phases (Fe, 1560 °C). The process of formation of native Fe (spheres of various sizes, loops, spongy iron), Fig. 2(a), due to redox reactions, is undoubtedly complex and is partially discussed in our publication (Persikov et al., 2019). Structure, composition and dimensions of the experimentally obtained metal phases (Fig. 2. and Table 2) are in good agreement with the natural data on the finds of small amounts of the metallic phase, primarily iron, found in igneous rocks of various composition and origin under the conditions of the Earth's crust (Oleynikov et al., 1985; Ryabov et al., 1985 and others). It has also been established that carbon, which is formed in experiments due to $CH_4$ pyrolysis, dissolves in the metal phase. Thus, the mechanism responsible for the presence of carbon in native iron in nature has been experimentally substantiated (Tomshin et al., 2023).

**Table 2.** Chemical compositions (wt. %) of metal phases in basalt melts (quenched samples) after hydrogen-methane fluid pressure experiments

| Components | № 2128 | № 2126 |
|---|---|---|
| Fe | 98.49 | 98.07 |
| Mo | no | 0.84 |
| Ti | 0.18 | 0.08 |
| O | 0.91 | 1.2 |
| Si | 0.1 | 0.16 |
| Ca | 0.0.8 | 0.23 |
| P | 1.03 | 0.52 |
| Sum | 100.79 | 101.1 |

**Note**: 1. The results presented in the table are averages of 7 dimensions. 2. The concentrations of all impurities (Si, Ca, Ti) in the metal phases are determined approximately, since these values are within the analytical errors.

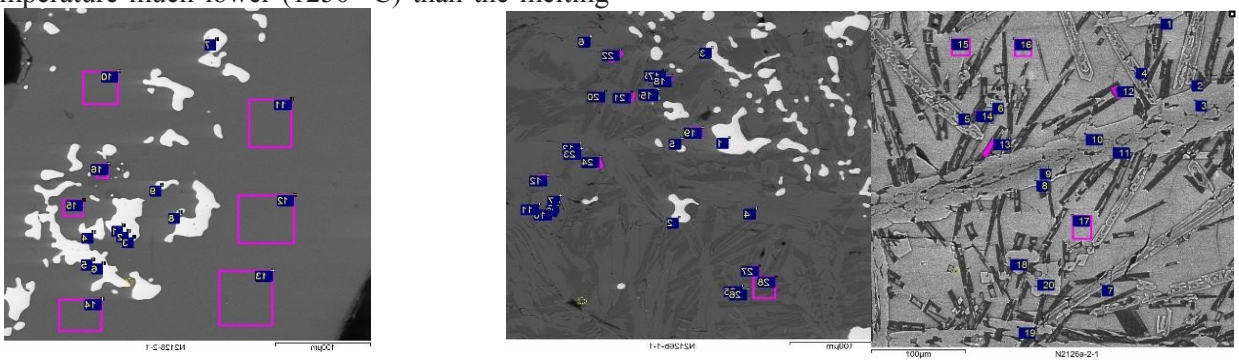

a) b) c)

**Fig. 2.** Raster micrographs in reflected electrons (BSE) of sample quenching products after experiments on interaction and crystallization of basalt melt under hydrogen- metan pressure.

(a) – experiment No 2128, experiment with melts of initial magnesian basalt, P(fl.) = 100 MPa, T = 1250 °C, duration of the experiment 1 hour, then reduction of fluid pressure to 10 MPa in isothermal mode, exposure for 1 hour, and then isobaric quenching (white color - metal alloy Fe, composition - see Table 2, black color - basalt glass, composition - see Table 1).
(b) – experiment No 2126, experiment on crystallization of magnesian basalt, P(fl.) = 100 MPa, T = 1250 °C, duration of the experiment 1 hour, then reduction of fluid pressure to 10 MPa in isothermal mode, holding for 1 hour, then temperature reduction to 1100 °C in isobaric mode, holding for 2 hours (crystallization) and then isobaric quenching (white color – metal alloy Fe, composition – see Table 2, light gray color-residual glass, composition-see. Table 1, black-gray color - crystals: olivine, clinopyroxene, plagioclase.
(c) - experiment No 2126, the result of crystallization of magnesian basalt melt (2,5,7-olivines; 3,10,11,18,19,20-clinopyroxenes; 12,13,14 – plagioclase; 15,16,17 – glass).

In crystallization experiments, it was found that the compositions of crystals (olivines, clinopyroxenes and plagioclase) formed in the experiment on crystallization of the magnesian basalt melt closely correspond to the compositions of crystals of lava flows of the Northern Eruption of the Tolbachik volcano in Kamchatka (Fig. 3). This result can be considered as an experimental confirmation of the participation of fluid ($CH_4$ + $H_2$) in a magmatic process, which is also consistent with the composition of the volcanic gases detected in the eruption of this volcano. It should be noted that metal-silicate liquation and the formation of a metallic phase of various textures established in experiments are rare at this volcano (Fedotov et al., 1984). If we take into account that crystallization was carried out at a fluid pressure of 10 MPa, it is likely that in nature the metallic phase was oxidized when magma rose from the magma chamber under the volcano to the surface.

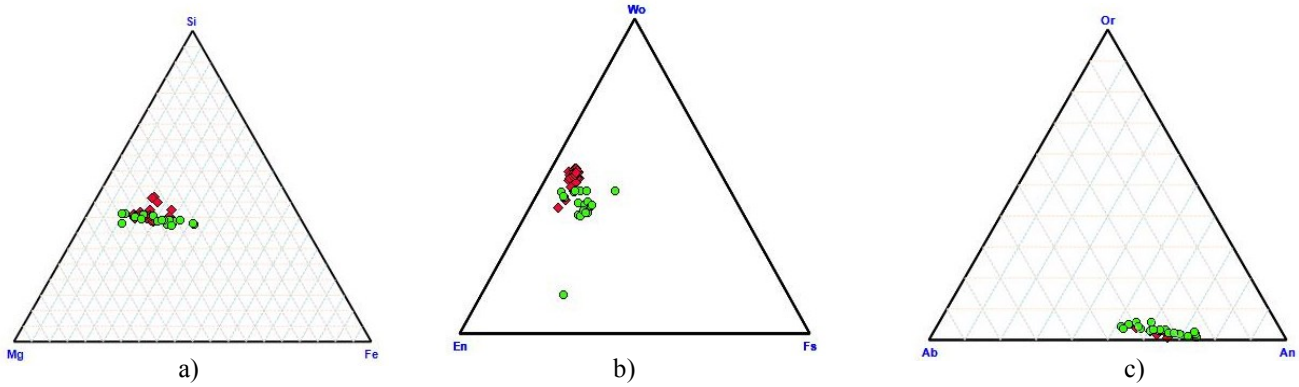


**Fig. 3.** Comparison of the composition of crystals formed in experiment No 2126 (red symbols) with the compositions of natural minerals from lava flows of magnesia basalt of the northern breakthrough of the Great Tolbachik eruption of 1975-1976, Kamchatka (Fedotov et al., 1984; green symbols).
(a) – olivines, experimental: Fo (max) = 86, Fo (min) = 65; natural: Fo (max) = 89, Fo (min) = 63;
(b) – clinopyroxenes, experimental: Wol = 49.64, En = 42.31, Fs = 8.06; natural: Wol = 49.64, En = 42.31, Fs = 8.06;
(c) – plagioclase – experimental: An = 62.24, Ab = 35.44, Or = 2.32; natural: An = 63.27, Ab = 33.77, Or = 2.97

**Conclusion.** Initially homogeneous basalt melt becomes heterogeneous when reacting and crystallizing under fluid pressure ($CH_4$ + $H_2$). As a result, the following phases are formed in the melt: more polymerized and silica-rich melts with some dissolved $H_2O$; small metal releases of liquation texture; olivine, clinopyroxene, and plagioclase (in the crystallization experiment). In addition, $H_2O$ is formed in the fluid phase (originally anhydrous fluid). It has been established that carbon, which is formed in experiments due to the pyrolysis of $CH_4$, dissolves in the metallic phase. Thus, the mechanism responsible for the presence of carbon in native iron in nature has been experimentally substantiated. The compositions of crystals (olivines, clinopyroxenes, and plagioclase) formed in the experiment on crystallization of magnesia basalt melt under the pressure of reducing fluid closely correspond to the compositions of crystals of lava flows of the Northern Eruption of Tolbachik volcano in Kamchatka.

***Sources of funding***. *The work was carried out within the framework of the research topic No FMUF-2022-0004 of the D.S. Korzhinsky Institute of Experimental Mineralogy of the Russian Academy of Sciences and the state assignment of IGEM RAS.*

**References**

Levashov, V.K., Okrugin, B.V. (1984) Estimation of physical conditions for the formation of native iron segregations in basalt melt. Geochemistry and mineralogy of basites and ultrabasites of the Siberian platform. Yakutsk: YAF SB AN SSSR, 54-62. (in Russian)

Oleynikov, B.V., Okrugin, A.V., Tomshin, M.D., et al. (1985) Native metal formation in platform basites. Ed. by V.V. Kovalsky. Yakutsk: YAF SB AN SSSR, 124 p. (in Russian)

E.S. Persikov, P.G. Bukhtiyarov, L.Ya. Aranovich A.N., Nekrasov, O.Yu. Shaposhnikova (2019) Experimental modeling of formation of native metals (Fe,Ni,Co) in the earth's crust by the interaction of hydrogen with basaltic melts. Geohemistry International, Vol. 57, No. 10, p. 1035–1044.

Persikov E.S., Bukhtiyarov P. G., Aranovich L. Y., Shchekleina M.D. Features of hydrogen interaction with basaltic melts at pressures 10-100 MP a and temperatures 1100-1250° C // Chem. Geol. 2020. V. 556. P. 116-119. https://doi.orgfl0.1016/j.chemgeo.2020.119829

Ryabov, V.V., Pavlov, A.L., Lopatin, G.G. (1985) Native iron of Siberian traps. Novosibirsk: Nauka SB RAN, 167 p. (in Russian)

Native Metals in Igneous Rocks (1985) All-Union Conference. Abstracts, Part 1. Ed. by B.V. Oleynikov. Yakutsk, Yaroslavl Branch of the Siberian Branch of

the USSR Academy of Sciences Publ., 188 p. (in Russian)
Tomshin M.D., Kopylova A.G., Vasilyeva A.E. Native iron in the traps of Siberia. Petrology. 2023. T. 31. № 2. Pp. 202-216.
Fedotov S.A. 1984. The Great Tolbachik Fissure Eruption of 1975-1976, Kamchatka Moscow: Nauka, 637 p. (in Russian)

## Suk N.I., Kotelnikov A.R., Nekrasov A.N., Neretina A.N. Experimental study of the solubility of molybdenite in aluminosilicate melts. *UDC 550.89:549.325.2*

IEM RAS, Chernogolovka, Moscow region
sukni@iem.ac.ru; kotelnik1950@yandex.ru

**Abstract.** The solubility of molybdenite ($MoS_2$) in aluminosilicate melts of varying alkalinity was experimentally studied at T = 900°C and P = 2 and 4 kbar under dry conditions and in the presence of 10 wt.% $H_2O$. Molybdenite solubility was found to depend on the composition of the aluminosilicate melt ((Na+K)/Al). In hydrous melts, sulfide sulfur is partially oxidized to sulfate sulfur, forming precipitates of alkaline (Na, K) sulfate melt with alkali molybdate inclusions. Feldspar crystals are observed in the glass around molybdenite crystals in dry melts with a glass agpaitic ratio of ~2.6 and in hydrous melts with a glass agpaitic ratio of ~1.4.

***Keywords**: molybdenite, aluminosilicate melt, experiment*

The solubility of molybdenite ($MoS_2$) in aluminosilicate melts of varying alkalinity was experimentally studied at T = 900°C and P = 2 and 4 kbar under dry conditions and in the presence of 10 wt.% $H_2O$. The experiments were conducted in a high-pressure gas vessel. The duration of the experiments was 10 days. The starting materials were melted granite glass of varying agpaiticity (1–2.5), as well as natural molybdenite. The composition of the experimental samples was determined by electron probe X-ray diffraction (EPXRD) analysis using a Tescan Vega II XMU scanning electron microscope (Tescan, Czech Republic) equipped with an INCA Energy 450 X-ray microanalysis system with an energy-dispersive (INCAx-sight) and crystal diffraction (INCA wave 700) X-ray spectrometer (Oxford Instruments, England) and the INCA Energy+ software platform. Analyses were performed using both the energy-dispersive (for rock-forming elements) and crystal diffraction (for Mo and S) spectrometers.

As a result of the experiments, glass columns containing molybdenite crystals were obtained. The compositions of the resulting experimental glasses are presented in Table 1. For a more accurate comparison, the glass analyses in dry systems are normalized to 100 wt.%, and in water-saturated systems to 95 wt.%.

It was found that the solubility of molybdenite depends on the composition of the aluminosilicate melt ((Na+K)/Al) (Fig. 1). In dry melts increase in the solubility of molybdenite is observed with an increase in the agpaitic ratio ((Na+K)/Al) of the aluminosilicate melt (Fig. 1). The $MoO_3$ content in the melt with $K_{agp}$>2 does not exceed 0.2 wt.%. A slight increase in the $MoO_3$ content is noted with a decrease in pressure from 4 kbar to 2 kbar.

**Table 1.** Glass compositions in molybdenite solubility experiments

| Oxides, wt% | Mo-5 | Mo-6 | Mo-7 | Mo-8 | Mo-9 | Mo-1 | Mo-2 | Mo-3 | Mo-4 |
|---|---|---|---|---|---|---|---|---|---|
| | Dry system | | Water-saturated system | | | Dry system | | | Water-saturated system |
| | T=900°C, P=4 kbar | | | | | T=900°C, P=2 kbar | | | |
| $SiO_2$ | 65.54 | 59.10 | 69.49 | 66.58 | 65.48 | 73.82 | 65.08 | 59.39 | 68.87 |
| $Al_2O_3$ | 13.59 | 14.21 | 13.13 | 14.21 | 14.32 | 13.45 | 13.57 | 14.23 | 13.01 |
| FeO | 0.14 | 0.15 | - | - | - | 0.20 | 0.18 | 0.16 | 0.17 |
| CaO | - | 0.16 | - | - | - | 0.15 | 0.16 | 0.22 | - |
| $Na_2O$ | 11.10 | 15.99 | 4.56 | 4.68 | 7.19 | 6.23 | 10.47 | 15.04 | 4.95 |
| $K_2O$ | 9.52 | 10.07 | 6.91 | 8.83 | 7.47 | 6.09 | 9.43 | 10.65 | 6.84 |
| $MoO_3$ | 0.08 | 0.18 | 0.81 | 0.61 | 0.39 | 0.02 | 0.09 | 0.19 | 0.91 |
| $SO_3$ | 0.03 | 0.15 | 0.12 | 0.09 | 0.15 | 0.05 | 0.10 | 0.12 | 0.25 |
| SUM | 100 | 100 | 95.00 | 95.00 | 95.00 | 100 | 100 | 100 | 95.00 |
| Kagp | 2.10 | 2.62 | 1.14 | 1.21 | 1.39 | 1.25 | 2.02 | 2.55 | 1.19 |

In the studied range of compositions, the dependence of the $MoO_3$ content in glass at T=900°C and P=2 kbar can be described by the equation:

$C_{MoO3}$, wt% = 0.09626-0.15502X+0.07521$X^2$, n=3, where X=(Na+K)/Al.

In water-saturated melts, partial oxidation of sulfide sulfur to sulfate sulfur occurs, forming alkaline sulfate melt precipitates with alkaline molybdate inclusions (Fig. 2). This indicates the development of liquid immiscibility between the silicate and sulfate melts. A sharp enrichment of the sulfate melts in molybdenum relative to the silicate melt is observed. The sulfate melt undergoes quench crystallization, forming quench phases: alkaline sodium sulfate, sodium and potassium sulfate in varying proportions, and sodium molybdate (sometimes with potassium admixture). The bulk composition of the sulfate melts at T=900°C and P=4 kbar is presented in Table 2. As a result, the system contains three phases: aluminosilicate melt, sulfate liquid, and molybdenite crystals. Consequently, in hydrous melts, an inverse relationship is observed between molybdenite solubility, which decreases with increasing melt agpaiticity. At $K_{agp}$<1.5, the molybdenum oxide content is ~0.4-0.8 wt.% (Fig. 1b). In the studied composition range, the dependence of the $MoO_3$ content in the glass can be described by the equation:

$C_{MoO3}$, wt.% = 13.08798-18.2254X+6.53968$X^2$, n=3, X=(Na+K)/Al.

A slight increase in the $MoO_3$ content is also noted with a decrease in pressure from 4 to 2 kbar (Fig. 1b).

In dry melts with a glass agpaitic ratio of ~2.6 and in hydrous melts with a glass agpaitic ratio of ~1.4, feldspar crystals are observed forming in the glass predominantly around molybdenite crystals (Fig. 3).

**Table 2.** Bulk compositions of sulfate melts at T=900°C and P=4 kbar

| Oxides, wt.% | Mo-7 | Mo-8 | Mo-9 |
|---|---|---|---|
| $Na_2O$ | 24.1 | 22.13 | 28.49 |
| $K_2O$ | 12.60 | 15.52 | 12.55 |
| CaO | 0.33 | 0.80 | 0.39 |
| $MoO_3$ | 29.27 | 28.73 | 25.44 |
| $SO_3$ | 30.90 | 30.15 | 30.48 |
| Sum | 97.20 | 97.31 | 97.33 |

*This work was supported by the IEM RAS Research Program No. FMUF-2022-0004.*

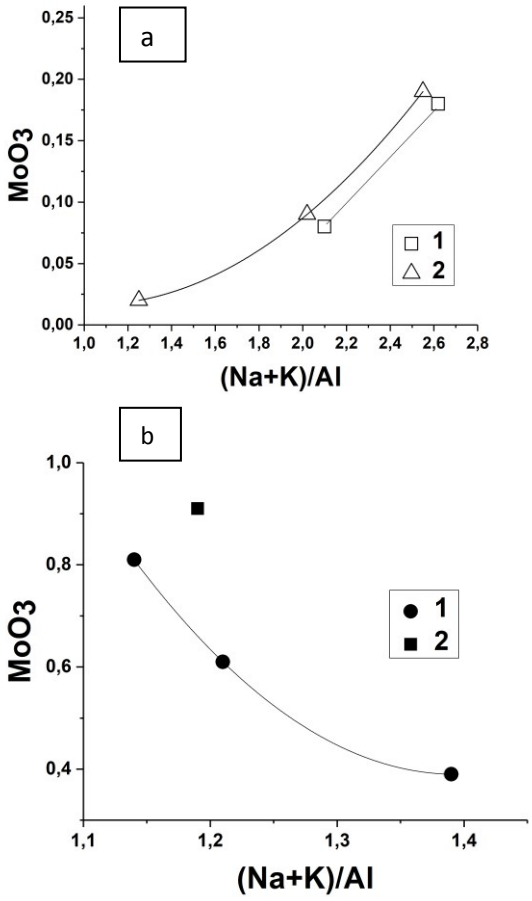


**Fig. 1**. Dependence of molybdenite solubility on the composition of the aluminosilicate melt (wt.%). a – in dry systems, b – in water-saturated systems; 1 – at T = 900°C and P = 4 kbar; 2 – at T = 900°C and P = 2 kbar

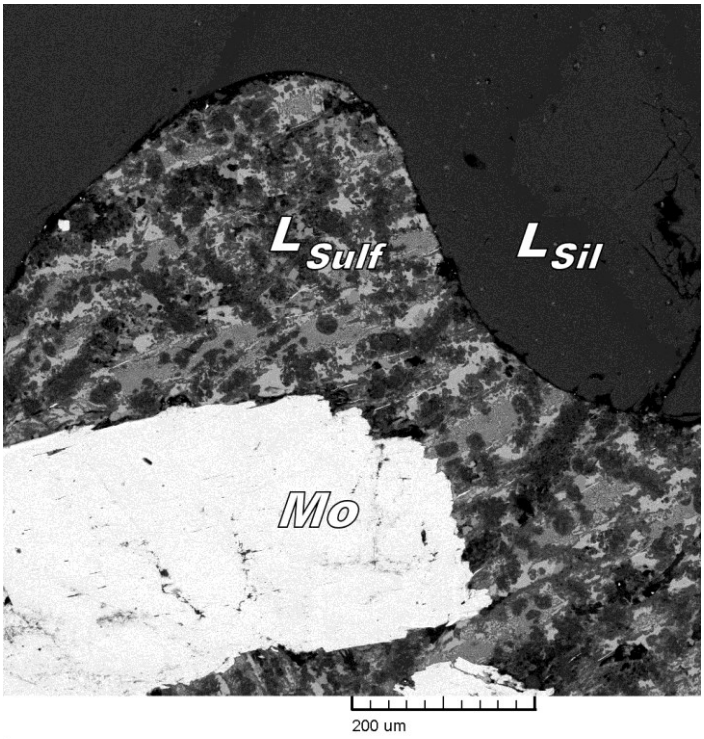


**Fig. 2.** Alkaline sulfate melt segregations in an aluminosilicate matrix with alkali molybdate inclusions at T = 900°C and P = 4 kbar in a hydrous system (sample Mo-9). $L_{Sil}$ – aluminosilicate melt, $L_{Sulf}$ – sulfate melt, *Mo* – molybdenite.

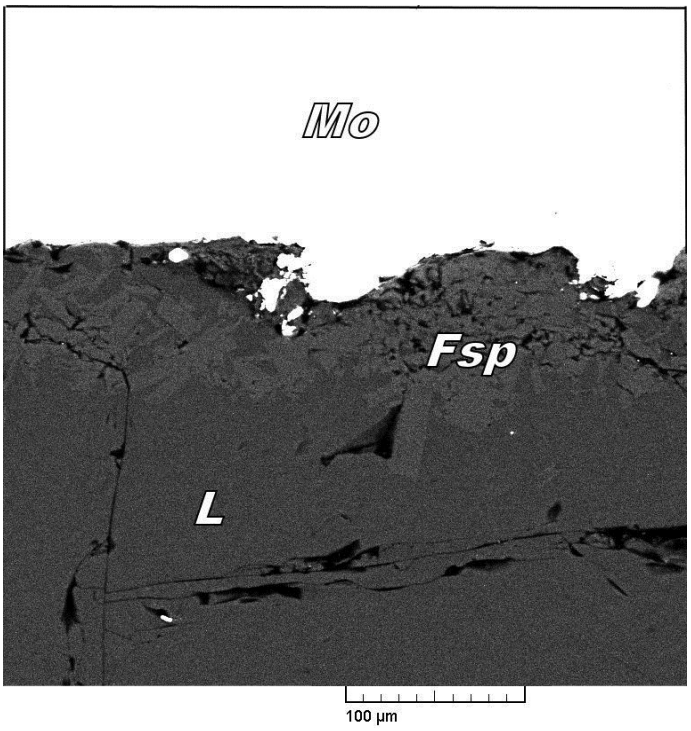


**Fig. 3**. Formation of feldspar crystals in glass around molybdenite crystals. (sample Mo-6). *L* – aluminosilicate melt, *Fsp* – feldspar, *Mo* – molybdenite.